

## Solid-State Single-Molecule Sensing with the Electronic Life-detection Instrument for Enceladus/Europa (ELIE)

**Authors:** Christopher E. Carr<sup>1,2\*+</sup>, José L. Ramírez-Colón<sup>2+</sup>, Daniel Duzdevich<sup>3-5</sup>, Sam Lee<sup>6</sup>, Masateru Taniguchi<sup>7</sup>, Takahito Ohshiro<sup>7</sup>, Yuki Komoto<sup>7</sup>, Jason M. Soderblom<sup>8</sup>, and M. T. Zuber<sup>8</sup>

### Affiliations:

<sup>1</sup> Daniel Guggenheim School of Aerospace Engineering, Georgia Institute of Technology, Atlanta, GA, 30332, USA. <sup>2</sup> School of Earth and Atmospheric Sciences, Georgia Institute of Technology, Atlanta, GA 30332, USA. <sup>3</sup> Massachusetts General Hospital, Department of Molecular Biology, Boston, MA 02114, USA. <sup>4</sup> Howard Hughes Medical Institute, Boston, MA 02114, USA. <sup>5</sup>Current address: Department of Chemistry, University of Chicago, 5735 S Ellis Avenue, Chicago, IL 60637. <sup>6</sup>MIT Department of Electrical Engineering and Computer Science, Cambridge, MA 02139, USA. <sup>7</sup>Osaka University, Institute of Scientific and Industrial Research, Osaka 565-0871 Japan. <sup>8</sup>MIT Department of Earth, Atmospheric and Planetary Sciences, Cambridge, MA 02139, USA.

<sup>+</sup>Co-first authors.

\*Correspondence to: [cecarr@gatech.edu](mailto:cecarr@gatech.edu). Address: ESM Building, Room G10, 620 Cherry St NW, Atlanta, GA 30332, USA

### One Sentence Summary:

A solid-state nanogap can determine the abundance distribution of amino acids, detect nucleic acids, and shows potential for detecting life as we know it and life as we don't.

## Abstract

Growing evidence of the potential habitability of Ocean Worlds across our Solar System is motivating the advancement of technologies capable of detecting life as we know it – sharing a common ancestry or common physicochemical origin to life on Earth – or don't know it, representing a distinct genesis event of life quite different than our one known example. Here, we propose the Electronic Life-detection Instrument for Enceladus/Europa (ELIE), a solid-state single-molecule instrument payload that aims to search for life based on the detection of amino acids and informational polymers (IPs) at the parts per billion to trillion level. As a first proof-of-principle in a laboratory environment, we demonstrate single-molecule detection of the amino acid L-proline at a 10  $\mu\text{M}$  concentration in a compact system. Based on ELIE's solid-state quantum electronic tunneling sensing mechanism, we further propose the quantum property of the HOMO–LUMO gap (energy difference between a molecule's highest energy occupied molecular orbital and lowest energy unoccupied molecular orbital) as a novel approach to measure amino acid complexity. Finally, we assess the potential of ELIE to discriminate between abiotically and biotically derived  $\alpha$ -amino acids in order to reduce false positive risk for life detection. Nanogap technology can also be applied to the detection of nucleobases and short sequences of IPs such as, but not limited to, RNA and DNA. Future missions may utilize ELIE to target preserved biosignatures on the surface of Mars, extant life in its deep subsurface, or life or its biosignatures in the plume, surface, or subsurface of ice moons such as Enceladus or Europa.

**Key words:** Life detection; Europa; Enceladus; Mars; biosignatures; amino acids; solid-state nanogaps; mechanically controlled break junction; HOMO–LUMO gap.

## **Main Text:**

### **1. Introduction**

Widespread synthesis of complex organics (amino acids, nucleobases, sugars) occurred early in the history of the solar nebula due to radiation processing of ices (Ciesla and Sandford 2012; Nuevo *et al.* 2012; Nuevo *et al.* 2009; Meinert *et al.* 2016), which is likely to occur throughout the universe. These building blocks of “life as we know it” are believed to have been delivered to all potentially habitable zones in the Solar System by comet and meteorite impacts (Schmitt-Kopplin *et al.* 2010; Engel and Macko 1997; Cooper *et al.* 2011; Martins *et al.* 2008; Callahan *et al.* 2011). Life might have arisen under similar physicochemical environments, such as within alkaline vent systems (Martin and Russell 2007; Martin *et al.* 2008) or impact-driven hydrothermal systems (Osinski *et al.* 2013) on the early Earth, Mars, or within subsurface oceans on icy worlds (Vance *et al.* 2007; Russell *et al.* 2014; Barge and White 2017). Because these building blocks form in interstellar space (Ciesla and Sandford 2012; Nuevo *et al.* 2012; Nuevo *et al.* 2009), in reducing planetary atmospheres (Hörst *et al.* 2012), and through aqueous chemistry (Ménez *et al.* 2018; Steel *et al.* 2017), we hypothesize that amino acids (AAs) are a common component of life, and that nucleic acids or related informational polymers (IPs) might be a common solution for information storage and heredity.

Amino acids can be stable over geologic time (Pizzarello and Cronin 2000; Glavin *et al.* 1999; Bada *et al.* 1998; Engel and Macko 1997), and the structural complexity and abundance distribution that has been measured from extraterrestrial material, as well as under terrestrial abiotic production, represents a null hypothesis for amino acid distributions in the search for ancient or extant life (Davila and McKay 2014; Reh *et al.* 2016). Quantum chemical calculations and biochemical experiments have further shown that the chemical reactivity of proteinogenic

amino acids exhibits a notable pattern related to their temporal emergence in the genetic code (Granold *et al.* 2018); amino acids added later into the genetic code have greater reactivity than those found in the Murchison meteorite or recovered from the Miller-Urey experiment, which coincide with those that are predicted to have been added early (Trifonov 2009). Thus, as we discuss later, this property can be utilized as a new measure of amino acid complexity and possibly as an indicator of life that utilizes regulated electron transfer mechanisms. Therefore, the detection of amino acids, along with their abundance distribution, can be used as a potential biosignature that would allow for the differentiation between widespread abiotic chemistry and potentially ancient or extant life. Alternatively, charged backbones, like the polyphosphates of DNA and RNA, are likely universal for aqueous life (Benner 2017; Benner 2004): they separate a polymer's physical properties from its associated information content, facilitating replication and evolution. Quantifying the presence of linear charged polymers with encoded information content could provide evidence of life, even without knowing the structure of the informational units (such as nucleobases) or their sequence. However, recent work demonstrating abiotic synthesis of RNA polymers 100-300 nucleotides in length on mineral glass surfaces demonstrates the potential for linear charged polymers in a prebiotic setting (Jerome *et al.* 2022).

Life elsewhere may also use similar building blocks because of shared ancestry through meteoritic exchange, a scenario most plausible for Earth and Mars (Carr 2022; Fritz *et al.* 2005; Shuster and Weiss 2005; Weiss *et al.* 2000; Gladman and Burns 1996a; Gladman *et al.* 1996b). Instruments targeting RNA or DNA, such as the Search for Extra-Terrestrial Genomes (SETG) (Ruvkun *et al.* 2002; Carr *et al.* 2016; Lui *et al.* 2011; Isenbarger *et al.* 2008a; Isenbarger *et al.* 2008b) are in development, but rely on biological reagents that must be stabilized, and require a complex series of steps to prepare nucleic acids for analysis. Solid-state nanopores have

demonstrated the detection and characterization of nucleic acids, and have been proposed to potentially detect other polymers (Rezzonico 2014; Xia *et al.* 2022). However, at present, such nanopores require high (MHz) sample rates and ultra-low noise, and even so, solid-state nanopore detection of individual bases has not yet been realized (Shekar *et al.* 2016).

Here we propose the Electronic Life-detection Instrument for Enceladus/Europa (ELIE), a solid-state single-molecule detector. ELIE relies on quantum electronic tunneling (QET) nanogap sensors (Figure 1), which can detect and discriminate among single  $\alpha$ -amino acids (Ohshiro *et al.* 2014), and detect RNA and DNA, including individual bases and, with caveats, short oligonucleotide sequences (Ohshiro *et al.* 2018; Ohshiro *et al.* 2012). We aim to primarily target amino acids and IPs, although we are developing ELIE with the potential to target other types of molecules, including abiotic or prebiotic polymers (Figure 2). This versatility of detecting a wide array of molecules would allow ELIE identify forward contamination, but also ancestrally related life – and possibly mirror-image life or alternative polymers. Here we focus on amino acid detection because amino acids exhibit relatively high stability under harsh conditions in comparison to IPs, and are potential targets for characterizing abiotic and prebiotic environments, and classifying ancient or extant life.

The discovery of Enceladus' plume of icy grains and gas by the Cassini mission (Porco *et al.* 2006; Waite Jr *et al.* 2009) and the tentative evidence for transient water vapor plumes at several locations on Europa found in Hubble Space Telescope observations (Roth *et al.* 2014; Sparks *et al.* 2016), support the idea of material transport from the interior of these moons and, in concert with other studies, the presence of global subsurface oceans (Kivelson *et al.* 2000; Thomas *et al.* 2016; Zimmer *et al.* 2000). Based on known amino acids degradation rates, previous works suggest that a detection of amino acids in these predicted subsurface oceans

above a concentration of 1 nM would indicate active production by geochemical or biotic pathways (Truong *et al.* 2019). Additionally, Steel *et al.* 2017 predict that methanogen-based microbial life and abiotic hydrothermal processes could produce a maximum of 90  $\mu\text{M}$  and 104  $\mu\text{M}$  concentrations of amino acids, respectively, in the predicted subsurface oceans of these moons.

In this study, we validate the single-molecule detection of L-proline with our first low-technology readiness level (TRL) ELIE prototype, and use this result to extrapolate an order-of-magnitude sensitivity of 1 nM. Furthermore, we provide evidence that the quantum property of the HOMO–LUMO gap describes the physical mechanisms underlying the conductance patterns of different proteinogenic amino acids obtained from the solid-state single-molecule detector. Using amino acid abundance distributions reported in the literature, we then show the potential for ELIE to discriminate between abiotically and biotically derived  $\alpha$ -amino acids. Finally, this work provides preliminary evidence for the feasibility of integrating ELIE into future *in-situ* life detection missions.

## **2. Methods**

### *2.1. ELIE Instrument Hardware*

The starting point for ELIE was a benchtop nanogap system developed by the Taniguchi laboratory at Osaka University as reported in Tsutsui *et al.* 2008a, Ohshiro *et al.* 2012, Ohshiro *et al.* 2014, and Ohshiro *et al.* 2018 (Figure 3a). The benchtop system consists of a picoammeter, a National Instruments (NI) computer, a custom Faraday cage enclosing stepping and piezo motors and a jig structure holding a nanogap chip, a piezo controller, and battery banks. One of the goals of the subsequently-developed ELIE prototype is to demonstrate a significant mass and volume reduction relative to this benchtop system. Compared to the benchtop system, the ELIE

system consists of a low-noise amplifier for voltage supply, a laptop for data collection, and a Faraday cage holding an amplifier head stage, a nanogap chip, and a manual micrometer (Figures 3b and 3c). The nanogap chips (Figure 3d) are fabricated as previously reported by Tsutsui *et al.* 2008a. First, a silicon substrate is spin-coated with a thin polyimide layer. Gold nanojunctions (100 nm x 100 nm) are then patterned on top using a standard electron-beam lithography and lift-off technique. Subsequently, the polyimide beneath the junction is carved away by isotropic reactive ion etching, using O<sub>2</sub>/CF<sub>4</sub> gas, to generate a free-standing gold nanowire bridge; this bridge is later formed into a nanometer-scale gap prior to measurement using the Mechanically Controlled Break Junction (MCBJ) method. An optional addition is a cover made of polydimethylsiloxane (PDMS), attached to the silicon substrate and treated with ozone plasma for bonding. This cover contains a microchannel that allows for the containment of a sample solution and its retention through reduced evaporation under room temperature conditions. The Faraday cage is connected to a low-noise and high-bandwidth amplifier (Chimera Instruments, VC100, 8 pA RMS at 100 kHz, with sampling up to 4 MHz) that supplies and controls the bias voltage (clamp  $\pm$  1V) and current measurements ( $\pm$ 20 nA) of the nanogap.

## 2.2. *ELIE Instrument Operation*

The chip is mounted in a three-point bending mechanism in a jig within the Faraday cage, rinsed with 10% ethanol (as a wetting agent) and bent mechanically with a manual micrometer to form an atomically sharp gap. A 10 k $\Omega$  resistor is connected in series to protect the nanogap junction from over-current breakdown due to ohmic heating while in the connected state. In order to form the nanogap, the chip is bent by the micrometer to an opened state while monitoring the current. Once the gap is formed and in the open (unconnected) state, the resistor is removed from the circuit so that the current resulting from the applied voltage difference will reflect the gap

conductance. As described by Tsutsui *et al.* 2008b, the resulting tunneling current ( $I$ ) can be defined as an exponential function of the gap distance ( $d$ ) as  $I \sim \exp(\beta d)$  with the decay constant  $\beta = -2\sqrt{2m\Phi}/\hbar$ , where  $m$  and  $\hbar$  are the electron mass and the work function of Au. The gap is typically characterized in a dry state or in the presence of a buffer prior to making measurements with a sample. The distance is adjusted by means of chip bending, which produces changes in the gap distance that are a fraction of the vertical motion of the adjustment mechanism. The distance is monitored by the (VC100) measured current, which represents the sum of offset error (set to zero when bias is set to 0 mV), ionic current, and tunneling current. In practice, the baseline is zeroed during analysis so that differences in current reflect enhancement of tunneling current when a molecule of interest occupies the gap.

### 2.3. *ELIE Instrument L-proline Measurement*

L-proline was obtained from Sigma (81709) and a 10  $\mu$ M L-proline solution prepared by dilution in nuclease free water with a background of 1 mM phosphate buffer, pH 7.4 at 25 °C (Sigma P3619). The solution was introduced through the microchannel and the current recorded for 5 minutes. Current measurements were conducted with an applied voltage of 100 mV and sampling rate of 4 MHz.

### 2.4. *ELIE Instrument Tunneling Current Data Analysis*

Data were low pass filtered to 25 kHz and downsampled to 100 kS/s in order to reduce the amount of electrical noise and the amount of data storage, respectively. Baseline adjustment was defined by estimating a kernel density over windows of 0.1 s with a 0.001 s sliding step. Events were detected using OpenNanopore v1.2, a tool that employs adaptive thresholding (by adjusting to low-frequency variations in the baseline) and a cumulative sum (CUSUM) fit to detect events (Raillon *et al.* 2012). Low-level noise signals within the set of events were subsequently



identified using a  $6\sigma$  threshold below the inferred mean of the events tunneling currents, and were excluded from further analysis. Features extracted from each of the events include the tunneling current (mean current level within single event) and dwell time (duration) (Figure 4a).

### *2.5. Linear Regression Models of Amino Acid Conductance and Dwell Time*

To gain insight into determinants of tunneling current and dwell time, linear regression models were fitted by plotting the values of various physical and quantum properties of proteinogenic amino acids (molecular weight, molecular volume, and HOMO–LUMO gap) against the conductance and dwell time values of amino acids measured by Ohshiro *et al.* 2014 (using the 0.55-nm and 0.70-nm-nanogap electrodes; refer to Figure S1). The HOMO–LUMO gap values of the proteinogenic AAs were reported by Granold *et al.* 2018 and determined by semiempirical calculations using the Molecular Orbital PACKage (MOPAC) 2003 AM1 Hamiltonian method in the MOPAC interface of Chem3D 9.0.

### *2.6. Predicting Differences in Distribution Patterns Between Meteoritic and Biologically Produced Amino Acids*

We generated a literature-based database of reported abundances of meteoritic  $\alpha$ -amino acids and amino acids extracted from diverse environmental samples (Elsila *et al.* 2021; Glavin *et al.* 2021; Aerts *et al.* 2020; Aponte *et al.* 2020; Glavin *et al.* 2020; Noell *et al.* 2018; Martins *et al.* 2015; Fuchida *et al.* 2014; Glavin *et al.* 2010; Hou *et al.* 2009; Martins *et al.* 2007). The analysis only considered meteoritic  $\alpha$ -amino acids observed in multiple meteorites samples and reported by multiple authors. The studied meteorites were grouped into groups and subgroups, following mineralogy and elemental and isotopic composition (Table S1). Environmental samples considered in the analysis cover some of the closest terrestrial analogs to the surface of Mars and predicted subsurface environments of Enceladus and Europa (Table S2). Estimated event rates

that would be expected for each amino acid by source (environmental or meteoritic) were determined by using an approximate standard event rate observed from the ELIE data in Section 2.4 of 50 events/s in 10  $\mu\text{M}$  aqueous solutions, and assuming a linear relationship between concentration and event rate. Finally, single-molecule conductance values of  $\alpha$ -amino acids reported by Ohshiro *et al.* 2014 (using the 0.70-nm-nanogap electrodes) were plotted against the predicted event rates. For the  $\alpha$ -amino acids not reported by Ohshiro *et al.* 2014, the expected nanogap conductance signals were estimated using the HOMO–LUMO gap regression model obtained in Section 2.5.

### 3. Results

#### 3.1. Proof of principle: Single-molecule detection of L-proline

Single-molecule detection was demonstrated with the ELIE system using 10  $\mu\text{M}$  L-proline aqueous solutions and manual adjustment of the gap size between the electrodes. Manual adjustment limited maintaining a gap in the unconnected state within a measurable gap size range to short intervals on the scale of seconds. The current–time profile obtained from this experiment is shown in Figure 4a. After low-pass filtering, downsampling, and further processing through the OpenNanopore v1.2 software tool, 203 events were detected across the 2.7 s signal. By subsequently applying a  $6\sigma$  threshold below the inferred mean of the event tunneling currents, 12 events were identified and removed, leaving 191 events to be analyzed (Figure 4b). As observed by the current and time histograms in Figure 4c and 4d, events detected had average current signals of  $40.21 \text{ pA} \pm 6.12 \text{ pA}$  and durations of  $2.33 \text{ ms} \pm 2.21 \text{ ms}$ . Extrapolation of this experimental result suggests a sensitivity of 1 nM or <100 ppt in 5 min, corresponding to 1 pmol/g. Lastly, the determined conductance was compared to measurements by Ohshiro *et al.* 2014 using the 0.55-nm and 0.70-nm-nanogap electrodes to test for L-proline.

Figure 4e suggests that the gap size was intermediate and closer to 0.70 nm. This results confirm the relationship between the gap distance and tunneling current previously outlined by Tsutsui *et al.* 2008b, where a larger gap distance generates lower tunneling currents, and therefore, conductance.

### 3.2. *Linear regression models*

A summary of the statistics obtained from the linear regression models, fitted by plotting conductance and dwell time values of amino acids against the specific amino acid's molecular weight, molecular volume and HOMO–LUMO gap, is found in Table S3. The HOMO–LUMO gap showed the best linear relationship to the conductance and dwell time values obtained by the 0.55-nm and the 0.70-nm-nanogap electrodes of all tested covariates. However, only the linear relationship observed between the HOMO–LUMO gap and the conductance values of amino acids obtained from the 0.70-nm-nanogap electrodes is interpreted as statistically significant (Figure 5). Figures S2 and S3 showcase the remaining linear regression plots obtained from Section 2.5.

### 3.3. *Predicted event rates of biotically and abiotically derived $\alpha$ -amino acids.*

The conductance-event rate plots of amino acids by sample and category predicts event rates with orders of magnitude higher for amino acids derived from the environmental samples in comparison to the amino acids derived from meteoritic samples (Figure S4). Furthermore, an overlap of estimated event rates is observed between all the higher HOMO–LUMO gap amino acids in the genetic code (Figure 6), which also coincide with those  $\alpha$ -amino acids found in meteorites, following the meteoritic reported amino acids gathered in the database.

## 4. Discussion

### 4.1. Nanogap technology for single-molecule detection and potential for space compatibility

Improving levels of detection towards single-molecule detection, in the pico-to femtomoles range, remains an ongoing goal for *in-situ* life-detection technologies. This is a significant issue because signatures of life or abiotically produced organics in other planetary bodies across our Solar System may be present at exceedingly low abundances, or only accessible in low abundances (Eigenbrode *et al.* 2021). Here, we demonstrate that the use of nanogap systems show great potential in this critical regard by performing as ultra-sensitive agnostic detectors without sacrificing the capacity to discriminate among molecules or chemical moieties (such as between different amino acids or DNA bases). Our extrapolated limit of detection meets thresholds proposed for organics in the Europa Lander notional Organic Compositional Analyzer baseline payload (Hand *et al.* 2017) and amino acids in the Enceladus Orbilander notional separation mass spectrometer and microcapillary electrophoresis with laser-induced fluorescence (MacKenzie *et al.* 2021). In comparison to other state-of-the-art instruments, such as gas chromatography-mass spectrometry (GC-MS) or capillary electrophoresis coupled to laser-induced fluorescence (CE-LIF), nanogap systems do not require derivatization agents to enable sensitive detection and separation of the targeted biomarkers. Many derivatization agents have shown preferential reactions with water that produce increased background signals and low derivatization efficiencies of the targeted molecules (Goesmann *et al.* 2017; Leshin *et al.* 2013) and/or form by-products that interfere with the targeted molecules at low concentrations (Stalport *et al.* 2012; Creamer *et al.* 2017). Furthermore, the nanogap adjustment mechanism provides a general detection approach of nanometer-scale molecules

(e.g., individual amino acids) or moieties (e.g., nucleobases) that are part of longer biomarkers, such as peptides, nucleic acids, or other polymers.

#### 4.2. HOMO–LUMO gap as indicator of amino acid biogenicity

Linear regression models, obtained by using data of single-molecule conductance measurements from nanogap sensing experiments of single amino acids (Ohshiro *et al.* 2014), demonstrated a relationship between the level of conductance and the HOMO–LUMO gap values of 8 proteinogenic amino acids at higher nanogap sizes. Higher conductance values are obtained for amino acids with lower HOMO–LUMO gap values; a quantum property that defines the energy difference between a molecule’s highest energy occupied molecular orbital (HOMO) and lowest energy unoccupied molecular orbital (LUMO) in ground state. This may reflect the importance of electron transfer as an evolutionary adaptation of life as we know it; electron transfer pathways are essential for metabolism, biosynthesis, metal ligation, and counteracting biochemical changes in the environment, such as the rising oxygen concentrations within cells that initially evolved to thrive in anoxic environments (Cavalier-Smith 2006; Weiss *et al.* 2016; Moosmann 2021). Such potential molecular adaptations also correlate with various thermodynamic properties of amino acids within the genetic code: posited late additions of amino acids to the genetic code may have enabled increasingly reactive proteins to act as organic semiconductors (Figure 7), mediated by the incorporation of aromatic systems and less electronegative heteroatoms into their structures (Figure 8) (Bender *et al.* 2008; Gray and Winkler 2015).

From a quantum physical context, the relationship between the level of conductance and the HOMO–LUMO gap in solid-state single-molecule detectors is attributed to the electron transport mechanism behind single-molecule junctions. The band structures of the gold

nanojunctions within the nanogap chip are composed of crystal orbitals that conduct electrons at the Fermi level, a continuous energy level at room temperature (Taniguchi, 2017). Once these orbitals interact with another molecule passing through the nanogap, electronic interactions occur, shifting electron transmission within the nanogap and, in turn, generating changes in the conductance band that are mainly dependent on the conformation of the molecule. Molecules with lower HOMO–LUMO gaps tend to have their HOMO orbitals overlapping to a greater extent with the Fermi level of the nanoelectrodes, thus permitting a greater electron transmission (Taniguchi 2019). Therefore, this quantum property of amino acids explains the trends observed in the resulting conductance of amino acids sensed by the nanogap system. Consequently, the HOMO–LUMO gap is an accurate predictor of amino acid conductance, and thus amino acid complexity, in nanogaps systems at nanogap sizes that are significantly higher than the targeted molecules (Figures 5). In contrast, this relationship is not true for mass and spatial size (molecular volume), which seem to be the determining mechanisms responsible of electrical sensing (via ionic current blockade) in biological and solid-state nanopores (Wei *et al.* 2020).

In contrast, no statistically significant relationship was observed between the dwell time from the nanogap sensing experiments of single amino acids by Ohshiro *et al.* 2014 and the proteinogenic amino acid's physical and quantum properties considered in this study. However, as seen in Figure S5, there is an evident pattern in the dwell time at lower nanogap sizes, in which dwell time decreases in relation to the functional group of the amino acids tested. This can be related to the bonding strength between the gold nanoelectrodes and the anchoring group of the amino acid. It has been previously reported that thiol and amine groups form strong-stable and weak-covalent bonds on gold surfaces, respectively (Xue *et al.* 2014; Leff *et al.* 1996). Furthermore, imidazole groups are known to coordinate to gold nanoparticles and contribute

significantly to interactions between metallic surfaces and biological filaments (Zhou *et al.* 2010). These observations suggest that the bond strength between the gold atoms and amino acids like histidine, cysteine, and lysine allow for longer periods of single-molecular junctions at low nanogap sizes. Further studies are needed to assess other factors (e.g. electrical potential, molecular volume) and their possible combinatory influence on the dwell time at longer nanogap sizes. These results also highlight the need for automated gap control in order to maintain the gap at optimal distances for the molecular junction to be formed with the targeted molecules.

#### *4.3. ELIE's potential for discrimination between biotically and abiotically derived $\alpha$ -amino acids.*

Detection of low HOMO–LUMO gap small molecules may be indicative of life, but such molecules are not unique to living systems. Some amino acids in the genetic code with lower HOMO–LUMO gaps ( $<10$  eV;  $5\sigma$  below the mean HOMO–LUMO gap of Murchison meteorite amino acids, as reported by Granold *et al.* 2018) have been reported to be produced abiotically in terrestrial environments and endogenously in extraterrestrial materials. Ménez *et al.* 2018 demonstrated the abiotic formation of tryptophan, an aromatic  $\alpha$ -amino acid with a low HOMO–LUMO gap, during hydrothermal alteration of mantle rock in the Atlantis Massif. Moreover, Friedel-Crafts-type reactions are predicted to be responsible for the formation of this amino acid during the hydrothermal alteration of oceanic peridotites; a different pathway from the Strecker-cyanohydrin synthesis, which has been predominantly supported for the formation of endogenous  $\alpha$ -amino acids in CM and CR chondrites (Martins *et al.* 2007; Ehrenfreund and Charnley 2000; Glavin *et al.* 2020).

ELIE will be able to provide the abundance distributions of  $\alpha$ -amino acids within the sample, and thereby assess the abiotic or biotic origin of these targeted molecules. Because the

abiotic production of amino acids is thermodynamically driven (Higgs and Pudritz 2009), lower molecular weight amino acids, with lower values of Gibbs free energy of formation (Figure 8), are often found in high abundances within abiotic samples (Figure S6). Biotic production, on the other hand, is driven by functionality, yielding higher abundances of high molecular weight species with low HOMO–LUMO gaps (e.g. phenylalanine and tyrosine) relative to lower molecular weight amino acids. Therefore, if the mechanisms of formation mentioned above are ruled out, and the abundances of low HOMO–LUMO gap amino acids are high, then such detections (many events at high conductance) would be consistent with a potential biological source of amino acids or other small molecules.

#### 4.4. *Advancing ELIE*

Future work includes evaluating ELIE’s potential for detection of biomolecular mixtures, non-standard nucleic acid bases and other polymers in order to expand the structural diversity scope of detection and reduce the risk of false negatives. This will allow the development of a biomolecule detection/characterization algorithm with the potential for molecule classification using supervised and unsupervised methods (Taniguchi *et al.* 2019). Furthermore, we seek to develop ELIE into a breadboard system with long-term expectations of being applicable to life detection missions in Ocean Worlds, satisfying the mass, power, and volume constraints needed for such missions. To reach these next steps, we are improving some of the instrument’s current limitations by (i.) integrating an automated piezoactuator for gap control, (ii.) optimizing the Mechanically Control Break Junction process, (iii.) characterizing gap quality through monitoring of quantized gap conductance, (iv.) automating sample handling, and (v.) reducing the size of the low-noise amplifier. These improvements will allow us to better assess the



performance of ELIE in relevant environments, including the influence of salt, vacuum exposure, vibration tolerance, and effects of space radiation.

## 5. Conclusions

The discovery of a second genesis of life on Europa or Enceladus would immediately suggest life is common in the universe, addressing fundamental questions, about life's origins and its distribution across the universe, that would change humanity's perspective. The present efforts are a proof of concept of an instrument capable of detecting single amino acids, at a sensitivity that is not currently feasible for most of the emerging technologies for *in-situ* amino acid detection proposed for planetary missions to Ocean Worlds. The detection of the amino acid L-proline was validated in the  $\mu\text{M}$  range, and extrapolation suggests an ultimate sensitivity in the pM range. Furthermore, the quantum property of HOMO–LUMO gap is shown to best describe the conductance levels of proteinogenic amino acids obtained by previous works, and thus, proposed as a novel approach to measure amino acid complexity. Finally, by predicting event rates based on amino acid distributions in terrestrial and extraterrestrial samples, we suggest a potential approach to distinguish between biotically and abiotically derived amino acid distributions. Ongoing efforts aim to extend ELIE's capabilities for detection of other biomolecules and to develop the instrument into a breadboard system for potential opportunities for infusion into Ocean Worlds missions.

**Acknowledgments:** We thank Bernd Moosmann for providing us the HOMO–LUMO gap data from the Murchison meteorite amino acids, the genetically encoded amino acids, and the various metabolic descendants of the shikimate pathway and the data of the peroxy radical scavenging assays. **Author contributions:** C.E.C. and J.L.R.C. conceived and wrote the paper; C.E.C.

collected the data; C.E.C. and S.L. built the hardware; M.T., T.O. and Y.L. provided the nanogap sensors; C.E.C and D.D. designed the L-proline experiment; all authors edited and approved the manuscript. **Author Disclosure Statement:** The authors declare no competing interests. **Funding:** This work was supported by NASA awards 80NSSC19K1028 and 80NSSC22K0188 to C.E.C.

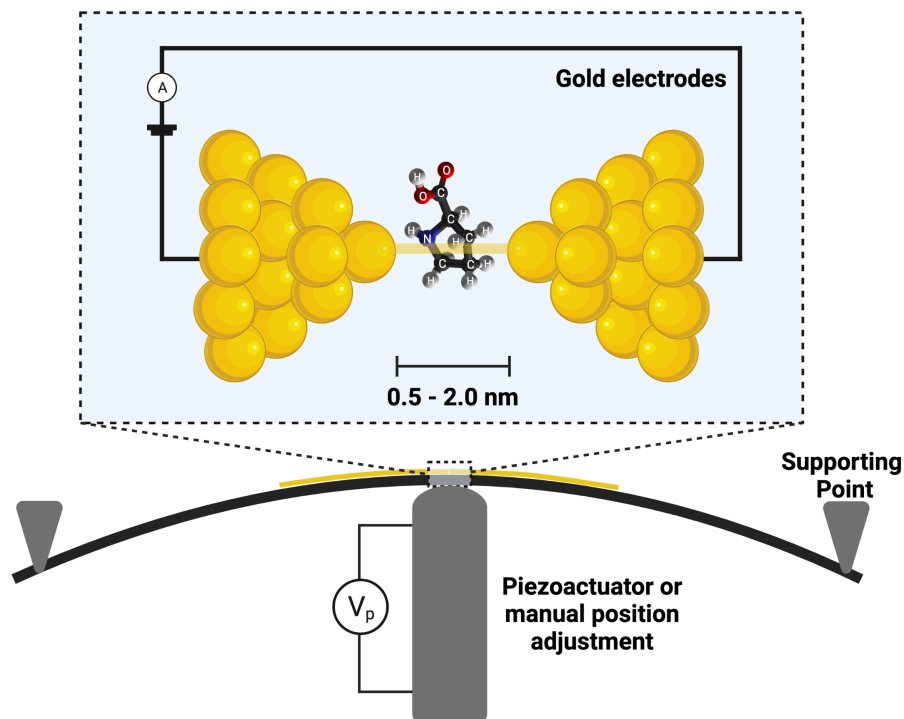


**Fig. 1. Single-molecule detection with a quantum electronic tunneling nanogap sensor, using the Mechanically Controlled Break Junction method.** A gold nanowire is mechanically broken by three-point bending, forming two gold nanoelectrodes. Additional adjustments of the actuator or manual micrometer change the gap size. Due to the dependency of electron tunneling upon the electronic structure of any intervening molecule, target molecules are detected by variations in electrical current between the electrodes (Di Ventra and Taniguchi 2016).

Decadal Survey Question	Goal	Objective	Investigation	Measurement Requirements: Physical Parameters	Measurement Requirements: Observables	Instrument Functional Requirements	Mission Functional Requirements
Decadal Priority Science Question 11: Is there evidence of past or present life in the solar system beyond Earth and how do we detect it?	Search for evidence of life on Enceladus and Europa	Detect and characterize any organic indicators of past or present life within Enceladus' plumes/surface/subsurface or Europa's surface	Characterize the amino acid composition of plume, surface or subsurface materials	Relative molar abundances of amino acid isomers. Distinguish between meteoritic and putative biogenic amino acids.	Molecular conductance and interaction times & frequency of 0.4–2 nm-diameter molecules and moieties & functional groups of larger molecules	Gap size: 0.5 to > 2 nm Sensitivity: 1000 pM in 5 min	Deliver 50 $\mu$ L of a liquid sample with relative low salt background (~ mM). Vibrations during operation to be determined. Faraday cage required to shield from EM noise. Operating temperature nominally 25 °C (full range not yet established but likely much wider).
			Search for evidence of genetic biopolymer in plume, surface or subsurface materials	Abundances of all amino acids detected relative to glycine-like amino acids (Gly). Sample's abundance vs. complexity distribution of amino acids as measured by their HOMO-LUMO gap.			
			Characterize other organic compounds of plume, surface or subsurface materials	Presence of a polyelectrolyte (polymer with a repeating charge in its backbone), such as DNA (ssDNA and dsDNA) and RNA (ssRNA, tRNAs, rRNAs).  Relative abundance and diversity of any (electronic structures of) organic functional groups, including whole molecules, molecular fragments and compounds potentially indicative of life (biomolecules and metabolic products) as low as 1 pmole/gram.			

**Fig. 2. ELIE Science Traceability Matrix.** Adapted for ELIE from goals of the Europa Lander Study Report and the Enceladus Orbilander Mission Concept (Hand *et al.* 2017; MacKenzie *et al.* 2021).

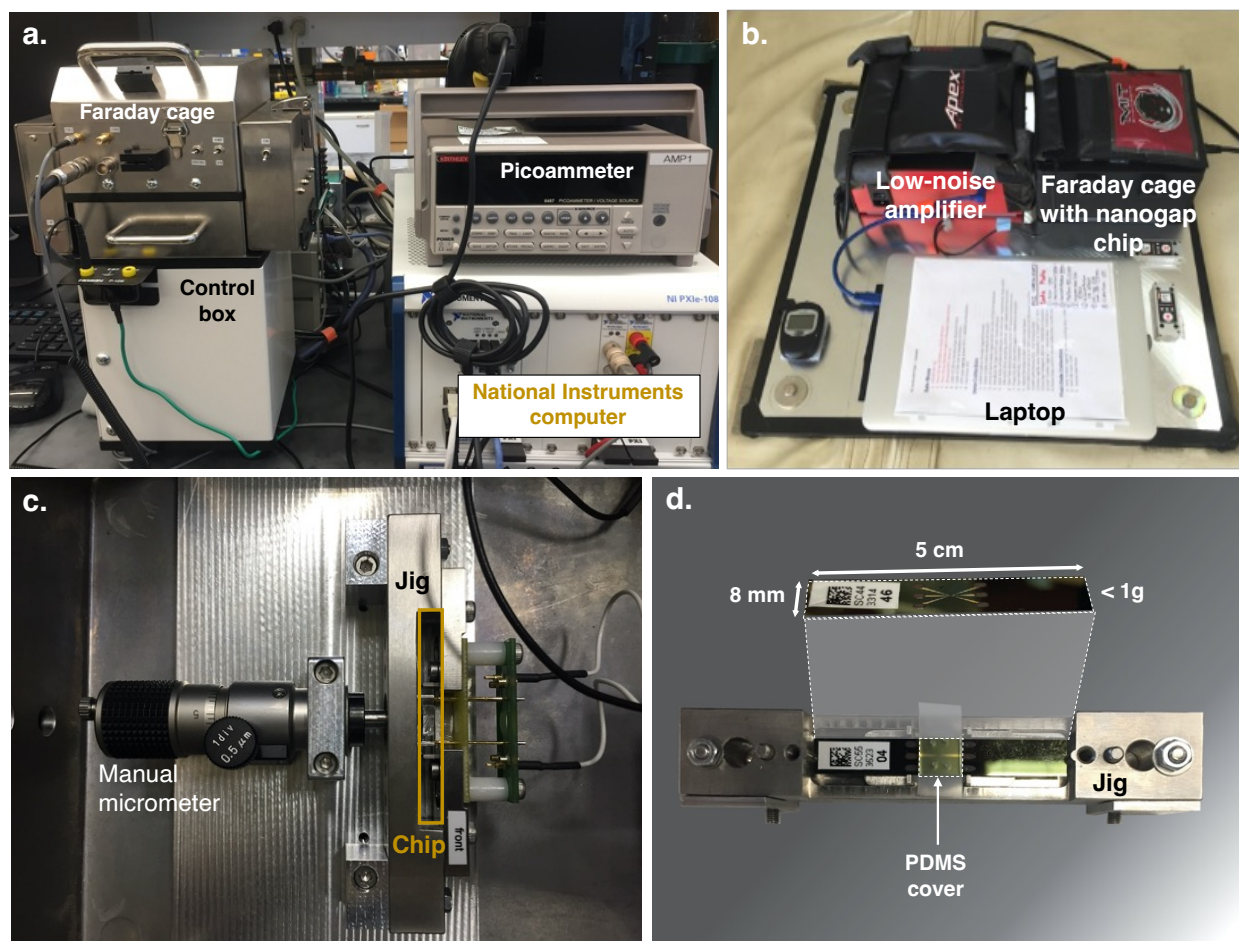


**Fig. 3. ELIE Instrument Prototype.** **a**, Benchtop Osaka University Nanogap System used for the analysis of amino acids in Ohshiro *et al.* 2014. **b**, Current system consisting of a laptop controlling the low-noise amplifier that, in turn, supplies and controls voltage to and within a Faraday cage that encloses **c**, a manual micrometer and jig structure holding the **d**, nanogap chip.

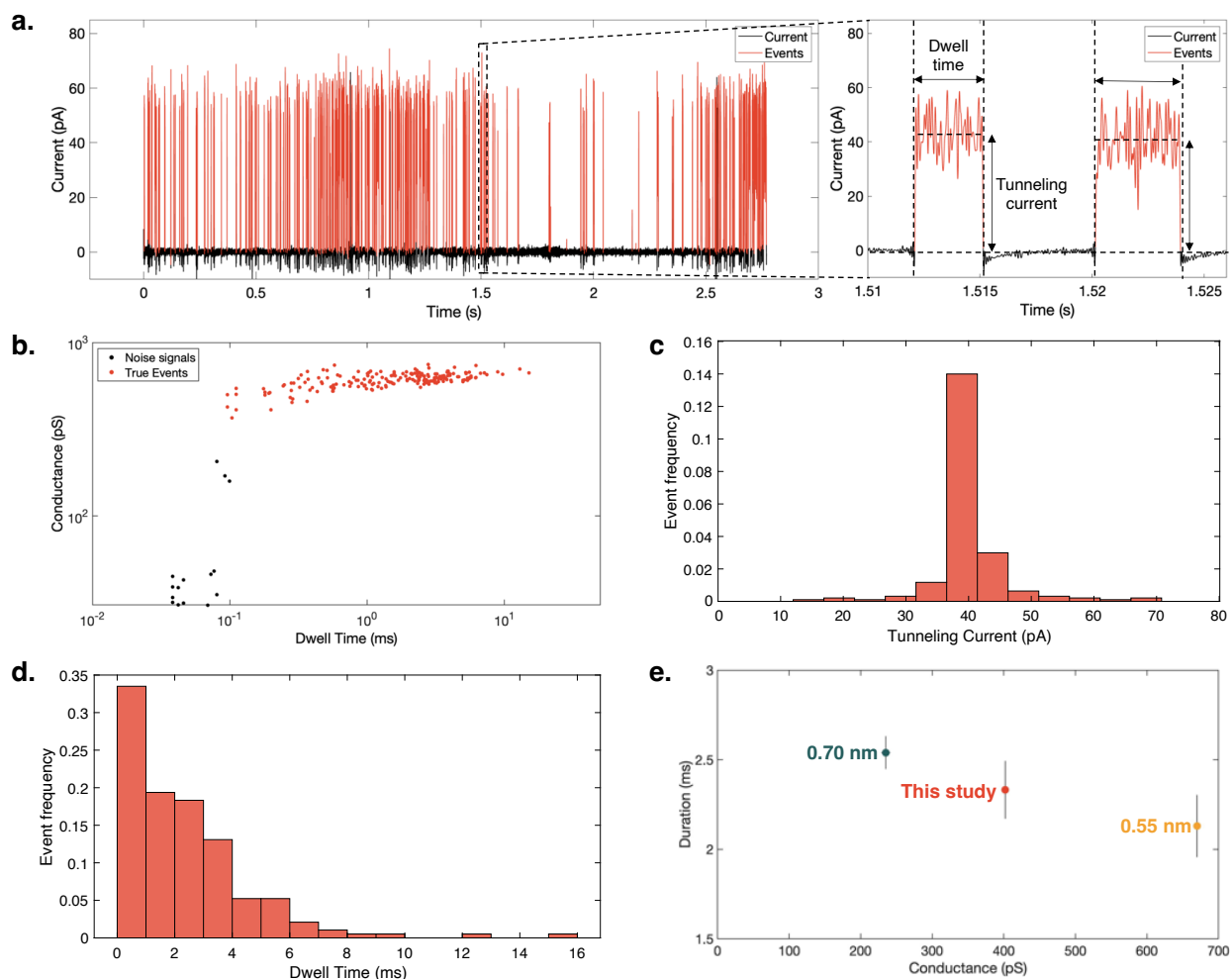


**Fig. 4. Single-molecule identification of L-proline.** **a**, Conductance–time profile of 10  $\mu$ M L-proline aqueous solution with an inset on the right showcasing the extracted features (dwell time and tunneling current) from each single event. **b**, Plot of single-molecule conductance and duration time of L-proline events displaying outliers within the data, identified by applying a  $6\sigma$  threshold below the inferred mean of the event tunneling currents. **c,d**, Conductance and dwell histograms of L-proline events. **e**, Plot of single-molecule mean conductance and mean duration time of L-proline events obtained from 0.7-nm- and 0.55-nm-nanogap-electrodes measurements in Ohshiro *et al.* 2014 and by manually adjusting ELIE’s chip nanogap size.

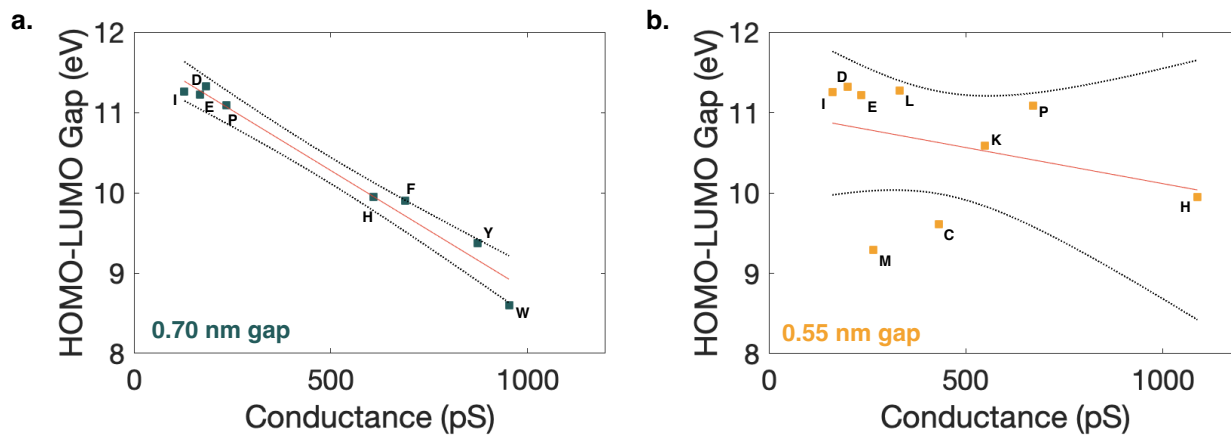


**Fig. 5. HOMO–LUMO gap of amino acids as a defining property for conductance levels using higher nanogap sizes. a,b,** Linear regression plots of conductance measurements of proteinogenic amino acids, obtained by Ohshiro *et al.* 2014 using 0.70-nm- and 0.55-nm-nanogap electrodes, respectively, against their HOMO–LUMO gap values (as reported by Granold *et al.* 2018). Refer to Figures S2 and S3, and Table S3 for the remaining linear regression plots and their statistical summary. Refer to Dataset S1 for the key to the one-letter amino acid designations of the amino acids studied by Ohshiro *et al.* 2014.

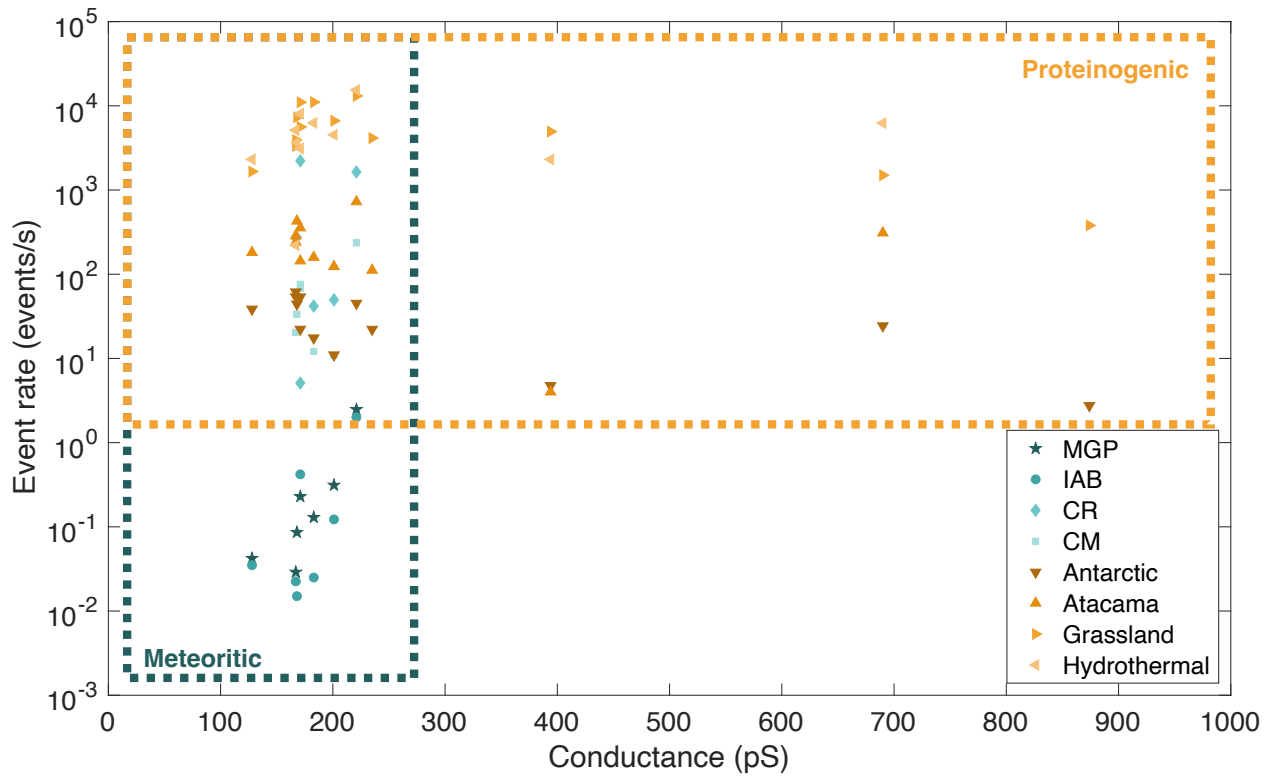


**Fig. 6. Potential discrimination between biotically and abiotically derived  $\alpha$ -amino acids.**

Distribution of predicted and experimentally validated conductance values of the 13 amino acids considered within the database as a function of the estimated event rates expected to be recorded from ELIE, on each of the meteorite (blue shades) and environmental (orange shades) samples. Meteorite group key: MGP (Main Group Pallasites); IAB (Iron meteorites group AB); CR (Renazzo-type chondrites); CM (Mighei-type chondrites).

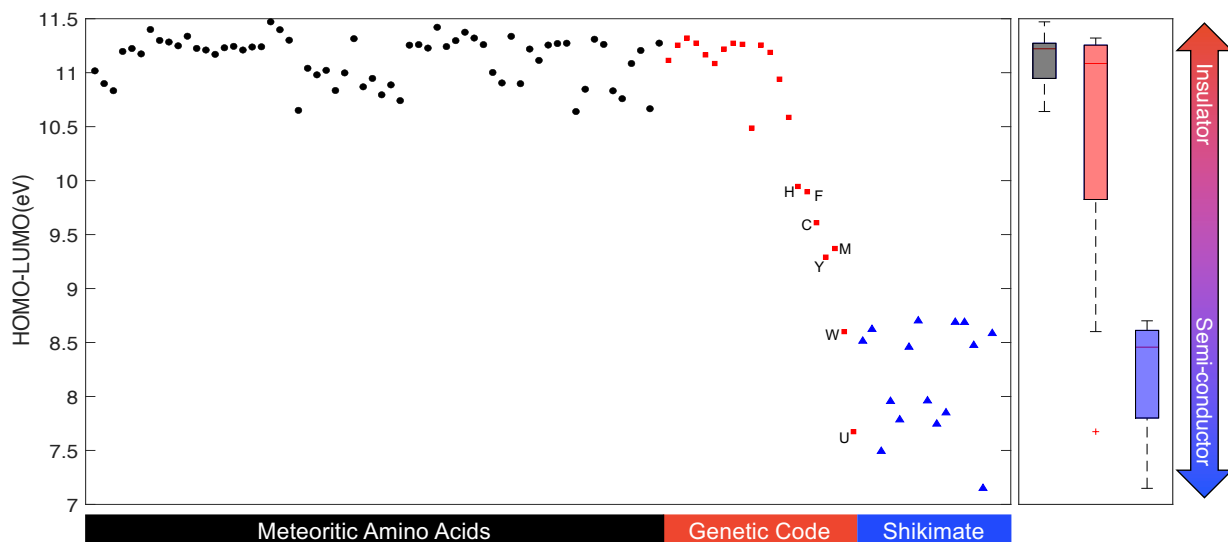


**Fig. 7. Amino Acid HOMO–LUMO gaps.** Distributions of the HOMO–LUMO gaps of 62 Murchison meteorite amino acids, 21 genetically encoded amino acids, and various metabolic descendants of the shikimate pathway (a biosynthetic pathway that leads to the formation of F, Y and W). The quantum-chemical properties were determined by Granold *et al.* 2018 using semiempirical calculations with the MOPAC2003 AM1 software package. The 21 proteinogenic amino acids (including selenocysteine) are plotted in the consensus order of their evolutionary appearance according to Trifonov 2009. Late additions to the genetic code are labeled with their respective one-letter code (H: histidine; F: phenylalanine; C: cysteine; M: methionine; Y: selenocysteine). Refer to Dataset S2 for individual names and HOMO–LUMO gaps of each amino acid and metabolic descendant of the shikimate pathway.



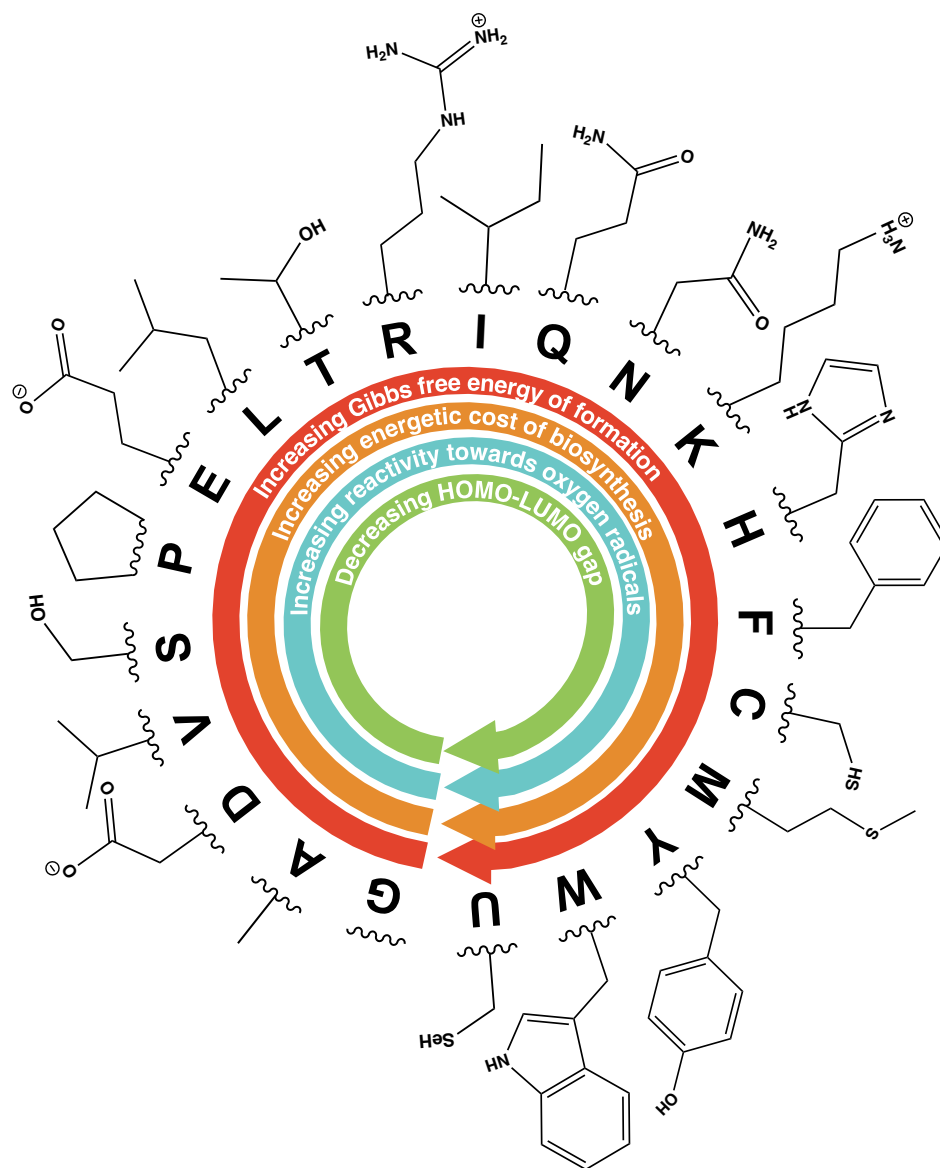


**Fig. 8.** Consensus order of appearance of proteinogenic amino acids within the genetic code as predicted by Trifonov 2009, along with their functional groups. Arrows are showing increasing and decreasing patterns of some AAs quantum, redox, and thermodynamic properties as discussed and reported by Akashi and Gojobori 2002, Amend and Shock 1998, and Granold *et al.* 2018. Arrows indicate trends with quantitative support (Figure S7). One letter amino acid designations are provided in the Dataset 3.

## 6. References

- Aerts J. W., Riedo A., Melton D. J., Martini S., Flahaut J., Meierhenrich U. J., Meinert C., Myrgorodska I., Lindner R., and Ehrenfreund P. (2020) Biosignature Analysis of Mars Soil Analogs from the Atacama Desert: Challenges and Implications for Future Missions to Mars. *Astrobiology*, 20: 766-784.
- Akashi H., and Gojobori T. (2002) Metabolic efficiency and amino acid composition in the proteomes of *Escherichia coli* and *Bacillus subtilis*. *Proceedings of the National Academy of Sciences*, 99: 3695-3700.
- Amend J. P., and Shock E. L. (1998) Energetics of amino acid synthesis in hydrothermal ecosystems. *Science*, 281: 1659-62.
- Aponte J. C., Elsila J. E., Hein J. E., Dworkin J. P., Glavin D. P., McLain H. L., Parker E. T., Cao T., Berger E. L., and Burton A. S. (2020) Analysis of amino acids, hydroxy acids, and amines in CR chondrites. *Meteorit Planet Sci*, 55: 2422-2439.
- Bada J. L., Glavin D. P., McDonald G. D., and Becker L. (1998) A search for endogenous amino acids in martian meteorite ALH84001. In: *Science*, American Association for the Advancement of Science, pp 362-365.
- Barge L. M., and White L. M. (2017) Experimentally Testing Hydrothermal Vent Origin of Life on Enceladus and Other Icy/Ocean Worlds. *Astrobiology*, 17: 820-833.
- Bender A., Hajieva P., and Moosmann B. (2008) Adaptive antioxidant methionine accumulation in respiratory chain complexes explains the use of a deviant genetic code in mitochondria. *Proceedings of the National Academy of Sciences*, 105: 16496-16501.
- Benner S. A. (2004) Understanding nucleic acids using synthetic chemistry. *Acc Chem Res*, 37: 784-97.

- Benner S. A. (2017) Detecting Darwinism from Molecules in the Enceladus Plumes, Jupiter's Moons, and Other Planetary Water Lagoons. In: *Astrobiology*, Mary Ann Liebert, Inc., publishers, pp 840-851.
- Callahan M. P., Smith K. E., Cleaves H. J., Ruzicka J., Stern J. C., Glavin D. P., House C. H., and Dworkin J. P. (2011) Carbonaceous meteorites contain a wide range of extraterrestrial nucleobases. In: *Proc Natl Acad Sci USA*, pp 13995-13998.
- Carr C. E. (2022) Resolving the History of Life on Earth by Seeking Life As We Know It on Mars. *Astrobiology*, 0: null.
- Carr C. E., Mojarro A., Tani J., Bhattaru S. A., Zuber M. T., Doebler R., Brown M., Herrington K., Talbot R., Fuller C. W. and others. (2016) Advancing the Search for Extra-Terrestrial Genomes. In: *IEEE Aerospace Conference*, pp 1-15.
- Cavalier-Smith T. (2006) Cell evolution and Earth history: stasis and revolution. *Philosophical Transactions of the Royal Society B: Biological Sciences*, 361: 969-1006.
- Ciesla F. J., and Sandford S. A. (2012) Organic synthesis via irradiation and warming of ice grains in the solar nebula. *Science*, 336: 452-4.
- Cooper G., Reed C., Nguyen D., Carter M., and Wang Y. (2011) Detection and formation scenario of citric acid, pyruvic acid, and other possible metabolism precursors in carbonaceous meteorites. *Proceedings of the National Academy of Sciences*, 108: 14015-14020.
- Creamer J. S., Mora M. F., and Willis P. A. (2017) Enhanced Resolution of Chiral Amino Acids with Capillary Electrophoresis for Biosignature Detection in Extraterrestrial Samples. *Anal Chem*, 89: 1329-1337.

- Davila A. F., and McKay C. P. (2014) Chance and Necessity in Biochemistry: Implications for the Search for Extraterrestrial Biomarkers in Earth-like Environments. In: *Astrobiology*, Mary Ann Liebert, Inc., publishers, pp 534-540.
- Di Ventra M., and Taniguchi M. (2016) Decoding DNA, RNA and peptides with quantum tunnelling. In: *Nat Nano*, Nature Publishing Group, pp 117-126.
- Ehrenfreund P., and Charnley S. B. (2000) Organic Molecules in the Interstellar Medium, Comets, and Meteorites: A Voyage from Dark Clouds to the Early Earth. *Annual Review of Astronomy and Astrophysics*, 38: 427-483.
- Eigenbrode J. L., Gold R., Canham J. S., Schulze E., Davila A. F., Seas A., Errigo T., Kujawa F., Kusnierkiewicz D., Lorentson C. and others. (2021) Contamination Control for Ultra-Sensitive Life-Detection Missions. *Frontiers in Space Technologies*, 2.
- Elsila J. E., Johnson N. M., Glavin D. P., Aponte J. C., and Dworkin J. P. (2021) Amino acid abundances and compositions in iron and stony-iron meteorites. *Meteoritics & Planetary Science*, 56: 586-600.
- Engel M. H., and Macko S. A. (1997) Isotopic evidence for extraterrestrial non-racemic amino acids in the Murchison meteorite. *Nature*, 389: 265-8.
- Fritz J., Artemieva N., and Greshake A. (2005) Ejection of Martian meteorites. *Meteoritics & Planetary Science*, 40: 1393-1411.
- Fuchida S., Mizuno Y., Masuda H., Toki T., and Makita H. (2014) Concentrations and distributions of amino acids in black and white smoker fluids at temperatures over 200°C. *Organic Geochemistry*, 66: 98-106.
- Gladman B. J., and Burns J. A. (1996a) Mars meteorite transfer: simulation. *Science*, 274: 161-2.

- Gladman B. J., Burns J. A., Duncan M., Lee P., and Levison H. F. (1996b) The Exchange of Impact Ejecta Between Terrestrial Planets. *Science*, 271: 1387-1392.
- Glavin D. P., Bada J. L., Brinton K. L. F., and McDonald G. D. (1999) Amino acids in the Martian meteorite Nakhla. In: *Proc Natl Acad Sci USA*, pp 8835-8838.
- Glavin D. P., Callahan M. P., Dworkin J. P., and Elsila J. E. (2010) The effects of parent body processes on amino acids in carbonaceous chondrites. *Meteoritics & Planetary Science*, 45: 1948-1972.
- Glavin D. P., Elsila J. E., McLain H. L., Aponte J. C., Parker E. T., Dworkin J. P., Hill D. H., Connolly Jr. H. C., and Laurretta D. S. (2021) Extraterrestrial amino acids and L-enantiomeric excesses in the CM2 carbonaceous chondrites Aguas Zarcas and Murchison. *Meteoritics & Planetary Science*, 56: 148-173.
- Glavin D. P., McLain H. L., Dworkin J. P., Parker E. T., Elsila J. E., Aponte J. C., Simkus D. N., Pozarycki C. I., Graham H. V., Nittler L. R. and others. (2020) Abundant extraterrestrial amino acids in the primitive CM carbonaceous chondrite Asuka 12236. *Meteoritics & Planetary Science*, 55: 1979-2006.
- Goesmann F., Brinckerhoff W. B., Raulin F., Goetz W., Danell R. M., Getty S. A., Siljestrom S., Missbach H., Steininger H., Arevalo R. D., Jr. and others. (2017) The Mars Organic Molecule Analyzer (MOMA) Instrument: Characterization of Organic Material in Martian Sediments. *Astrobiology*, 17: 655-685.
- Granold M., Hajieva P., Tosa M. I., Irimie F. D., and Moosmann B. (2018) Modern diversification of the amino acid repertoire driven by oxygen. *Proc Natl Acad Sci U S A*, 115: 41-46.

Gray H. B., and Winkler J. R. (2015) Hole hopping through tyrosine/tryptophan chains protects proteins from oxidative damage. *Proceedings of the National Academy of Sciences*, 112: 10920-10925.

Hand K. P., Murray A. E., Garvin J. B., Brinckerhoff W. B., Christner B. C., Edgett K. S., Ehlmann B. L., German C. R., Hayes A. G., Hoehler T. M. and others. (2017) Europa Lander Study 2016 Report – NASA's Europa Clipper. National Aeronautics and Space Administration.

Higgs P. G., and Pudritz R. E. (2009) A thermodynamic basis for prebiotic amino acid synthesis and the nature of the first genetic code. In: *Astrobiology*, pp 483-490.

Hörst S. M., Yelle R. V., Buch A., Carrasco N., Cernogora G., Dutuit O., Quirico E., Sciamma-O'Brien E., Smith M. A., Somogyi A. and others. (2012) Formation of amino acids and nucleotide bases in a Titan atmosphere simulation experiment. *Astrobiology*, 12: 809-17.

Hou S., He H., Zhang W., Xie H., and Zhang X. (2009) Determination of soil amino acids by high performance liquid chromatography-electro spray ionization-mass spectrometry derivatized with 6-aminoquinolyl-N-hydroxysuccinimidyl carbamate. *Talanta*, 80: 440-7.

Isenbarger T. A., Carr C. E., Johnson S. S., Finney M., Church G. M., Gilbert W., Zuber M. T., and Ruvkun G. (2008a) The most conserved genome segments for life detection on Earth and other planets. *Orig Life Evol Biosph*, 38: 517-33.

Isenbarger T. A., Finney M., Rios-Velazquez C., Handelsman J., and Ruvkun G. (2008b) Miniprimer PCR, a new lens for viewing the microbial world. *Appl Environ Microbiol*, 74: 840-9.

Jerome C. A., Kim H.-J., Mojzsis S. J., Benner S. A., and Biondi E. (2022) Catalytic Synthesis of Polyribonucleic Acid on Prebiotic Rock Glasses. *Astrobiology*, 22: 629-636.

- Kivelson M. G., Khurana K. K., Russell C. T., Volwerk M., Walker R. J., and Zimmer C. (2000) Galileo magnetometer measurements: a stronger case for a subsurface ocean at Europa. *Science*, 289: 1340-3.
- Leff D. V., Brandt L., and Heath J. R. (1996) Synthesis and Characterization of Hydrophobic, Organically-Soluble Gold Nanocrystals Functionalized with Primary Amines. *Langmuir*, 12: 4723-4730.
- Leshin L. A., Mahaffy P. R., Webster C. R., Cabane M., Coll P., Conrad P. G., Archer P. D., Atreya S. K., Brunner A. E., Buch A. and others. (2013) Volatile, Isotope, and Organic Analysis of Martian Fines with the Mars Curiosity Rover. *Science*, 341: 1238937.
- Lui C. S., Carr C. E., Rowedder H., Ruvkun G., and Zuber M. T. (2011) SETG: An instrument for detection of life on Mars ancestrally related to life on Earth. In: *2011 IEEE Aerospace Conference*, IEEE, Big Sky, USA, pp 1-12.
- MacKenzie S. M., Neveu M., Davila A. F., Lunine J. I., Craft K. L., Cable M. L., Phillips-Lander C. M., Hofgartner J. D., Eigenbrode J. L., Waite J. H. and others. (2021) The Enceladus Orbilander Mission Concept: Balancing Return and Resources in the Search for Life. *The Planetary Science Journal*, 2: 77.
- Martin W., Baross J., Kelley D., and Russell M. J. (2008) Hydrothermal vents and the origin of life. *Nat Rev Microbiol*, 6: 805-14.
- Martin W., and Russell M. J. (2007) On the origin of biochemistry at an alkaline hydrothermal vent. *Philos Trans R Soc Lond B Biol Sci*, 362: 1887-925.
- Martins Z., Alexander C. M. O. D., Orzechowska G. E., Fogel M. L., and Ehrenfreund P. (2007) Indigenous amino acids in primitive CR meteorites. *Meteoritics & Planetary Science*, 42: 2125-2136.

- Martins Z., Botta O., Fogel M. L., Sephton M. A., Glavin D. P., Watson J. S., Dworkin J. P., Schwartz A. W., and Ehrenfreund P. (2008) Extraterrestrial nucleobases in the Murchison meteorite. *Earth and Planetary Science Letters*, 270: 130-136.
- Martins Z., Modica P., Zanda B., and d'Hendecourt L. L. S. (2015) The amino acid and hydrocarbon contents of the Paris meteorite: Insights into the most primitive CM chondrite. *Meteoritics & Planetary Science*, 50: 926-943.
- Meinert C., Myrgorodska I., de Marcellus P., Buhse T., Nahon L., Hoffmann S. V., d'Hendecourt L. L. S., and Meierhenrich U. J. (2016) Ribose and related sugars from ultraviolet irradiation of interstellar ice analogs. In: *Science*, pp 208-212.
- Ménez B., Pisapia C., Andreani M., Jamme F., Vanbellingen Q. P., Brunelle A., Richard L., Dumas P., and Réfrégiers M. (2018) Abiotic synthesis of amino acids in the recesses of the oceanic lithosphere. In: *Nature*, Nature Publishing Group, pp 1.
- Moosmann B. (2021) Redox Biochemistry of the Genetic Code. *Trends Biochem Sci*, 46: 83-86.
- Noell A. C., Fisher A. M., Fors-Francis K., and Sherrit S. (2018) Subcritical water extraction of amino acids from Mars analog soils. *Electrophoresis*, 39: 2854-2863.
- Nuevo M., Milam S. N., and Sandford S. A. (2012) Nucleobases and prebiotic molecules in organic residues produced from the ultraviolet photo-irradiation of pyrimidine in NH<sub>3</sub> and H<sub>2</sub>O+NH<sub>3</sub> ices. *Astrobiology*, 12: 295-314.
- Nuevo M., Milam S. N., Sandford S. A., Elsila J. E., and Dworkin J. P. (2009) Formation of uracil from the ultraviolet photo-irradiation of pyrimidine in pure H<sub>2</sub>O ices. *Astrobiology*, 9: 683-95.



- Ohshiro T., Matsubara K., Tsutsui M., Furuhashi M., Taniguchi M., and Kawai T. (2012) Single-molecule electrical random resequencing of DNA and RNA. In: *Sci. Rep.*, Nature Publishing Group, pp 501.
- Ohshiro T., Tsutsui M., Yokota K., Furuhashi M., Taniguchi M., and Kawai T. (2014) Detection of post-translational modifications in single peptides using electron tunnelling currents. In: *Nat Nano*, Nature Publishing Group, pp 835.
- Ohshiro T., Tsutsui M., Yokota K., and Taniguchi M. (2018) Quantitative analysis of DNA with single-molecule sequencing. In: *Sci. Rep.*, Nature Publishing Group, pp 8517.
- Osinski G. R., Tornabene L. L., Banerjee N. R., Cockell C. S., Flemming R., Izawa M. R. M., McCutcheon J., Parnell J., Preston L. J., Pickersgill A. E. and others. (2013) Impact-generated hydrothermal systems on Earth and Mars. *Icarus*, 224: 347-363.
- Pizzarello S., and Cronin J. R. (2000) Non-racemic amino acids in the Murray and Murchison meteorites. In: *Geochimica et Cosmochimica Acta*, Pergamon, pp 329-338.
- Porco C. C., Helfenstein P., Thomas P. C., Ingersoll A. P., Wisdom J., West R., Neukum G., Denk T., Wagner R., Roatsch T. and others. (2006) Cassini Observes the Active South Pole of Enceladus. *Science*, 311: 1393-1401.
- Raillon C., Granjon P., Graf M., Steinbock L. J., and Radenovic A. (2012) Fast and automatic processing of multi-level events in nanopore translocation experiments. *Nanoscale*, 4: 4916-4924.
- Reh K., Spilker L., Lunine J. I., Aerospace J. W., and 2016. (2016) Enceladus Life Finder: The search for life in a habitable Moon - IEEE Conference Publication. In: *ieeexplore.ieee.org*

Rezzonico F. (2014) Nanopore-Based Instruments as Biosensors for Future Planetary Missions.

In: *Astrobiology*.

Roth L., Saur J., Retherford K. D., Strobel D. F., Feldman P. D., McGrath M. A., and Nimmo F.

(2014) Transient water vapor at Europa's south pole. *Science*, 343: 171-4.

Russell M. J., Barge L. M., Bhartia R., Bocanegra D., Bracher P. J., Branscomb E., Kidd R.,

McGlynn S., Meier D. H., Nitschke W. and others. (2014) The drive to life on wet and icy worlds. *Astrobiology*, 14: 308-43.

Schmitt-Kopplin P., Gabelica Z., Gougeon R. D., Fekete A., Kanawati B., Harir M., Gebefuegi

I., Eckel G., and Hertkorn N. (2010) High molecular diversity of extraterrestrial organic matter in Murchison meteorite revealed 40 years after its fall. *Proceedings of the National Academy of Sciences*, 107: 2763-2768.

Shekar S., Niedzwiecki D. J., Chien C.-C., Ong P., Fleischer D. A., Lin J., Rosenstein J. K.,

Drndic M., and Shepard K. L. (2016) Measurement of DNA Translocation Dynamics in a Solid-State Nanopore at 100 ns Temporal Resolution. In: *Nano Letters*, pp 4483-4489.

Shuster D. L., and Weiss B. P. (2005) Martian surface paleotemperatures from

thermochronology of meteorites. *Science*, 309: 594-600.

Sparks W. B., Hand K. P., McGrath M. A., Bergeron E., Cracraft M., and Deustua S. E. (2016)

PROBING FOR EVIDENCE OF PLUMES ON EUROPA WITH HST/STIS. In: *ApJ*, IOP Publishing, pp 121.

Stalport F., Glavin D. P., Eigenbrode J. L., Bish D., Blake D., Coll P., Szopa C., Buch A.,

McAdam A., Dworkin J. P. and others. (2012) The influence of mineralogy on recovering organic acids from Mars analogue materials using the “one-pot” derivatization experiment on the Sample Analysis at Mars (SAM) instrument suite. *Planetary and Space Science*, 67: 1-13.

- Steel E. L., Davila A., and McKay C. P. (2017) Abiotic and Biotic Formation of Amino Acids in the Enceladus Ocean. *Astrobiology*, 17: 862-875.
- Taniguchi M. (2019) Paving the way to single-molecule chemistry through molecular electronics. *Phys Chem Chem Phys*, 21: 9641-9650.
- Taniguchi M., Ohshiro T., Komoto Y., Takaai T., Yoshida T., and Washio T. (2019) High-Precision Single-Molecule Identification Based on Single-Molecule Information within a Noisy Matrix. *The Journal of Physical Chemistry C*, 123: 15867-15873.
- Thomas P. C., Tajeddine R., Tiscareno M. S., Burns J. A., Joseph J., Loredó T. J., Helfenstein P., and Porco C. (2016) Enceladus's measured physical libration requires a global subsurface ocean. *Icarus*, 264: 37-47.
- Trifonov E. N. (2009) The origin of the genetic code and of the earliest oligopeptides. *Res Microbiol*, 160: 481-6.
- Truong N., Monroe A. A., Glein C. R., Anbar A. D., and Lunine J. I. (2019) Decomposition of amino acids in water with application to in-situ measurements of Enceladus, Europa and other hydrothermally active icy ocean worlds. *Icarus*, 329: 140-147.
- Tsutsui M., Shoji K., Taniguchi M., and Kawai T. (2008a) Formation and self-breaking mechanism of stable atom-sized junctions. In: *Nano Lett.*, pp 345-349.
- Tsutsui M., Taniguchi M., and Kawai T. (2008b) Fabrication of 0.5 nm electrode gaps using self-breaking technique. *Applied Physics Letters*, 93: 163115.
- Vance S., Harnmeijer J., Kimura J., Hussmann H., Demartin B., and Brown J. M. (2007) Hydrothermal systems in small ocean planets. *Astrobiology*, 7: 987-1005.

- Waite Jr J. H., Lewis W. S., Magee B. A., Lunine J. I., McKinnon W. B., Glein C. R., Mousis O., Young D. T., Brockwell T., Westlake J. and others. (2009) Liquid water on Enceladus from observations of ammonia and  $^{40}\text{Ar}$  in the plume. *Nature*, 460: 487-490.
- Wei X., Ma D., Jing L., Wang L. Y., Wang X., Zhang Z., Lenhart B. J., Yin Y., Wang Q., and Liu C. (2020) Enabling nanopore technology for sensing individual amino acids by a derivatization strategy. *J Mater Chem B*, 8: 6792-6797.
- Weiss B. P., Kirschvink J. L., Baudenbacher F. J., Vali H., Peters N. T., Macdonald F. A., and Wikswo J. P. (2000) A low temperature transfer of ALH84001 from Mars to Earth. *Science*, 290: 791-5.
- Weiss M. C., Sousa F. L., Mrnjavac N., Neukirchen S., Roettger M., Nelson-Sathi S., and Martin W. F. (2016) The physiology and habitat of the last universal common ancestor. In: *Nature Microbiology*, Nature Publishing Group, pp 16116.
- Xia Z., Patchin M., McKay C. P., and Drndić M. (2022) Deoxyribonucleic Acid Extraction from Mars Analog Soils and Their Characterization with Solid-State Nanopores. *Astrobiology*, 22: 992-1008.
- Xue Y., Li X., Li H., and Zhang W. (2014) Quantifying thiol–gold interactions towards the efficient strength control. *Nature Communications*, 5: 4348.
- Zhou J. C., Wang X., Xue M., Xu Z., Hamasaki T., Yang Y., Wang K., and Dunn B. (2010) Characterization of gold nanoparticle binding to microtubule filaments. *Materials Science and Engineering: C*, 30: 20-26.
- Zimmer C., Khurana K. K., and Kivelson M. G. (2000) Subsurface Oceans on Europa and Callisto: Constraints from Galileo Magnetometer Observations. *Icarus*, 147: 329-347.

## Supplementary Data

### **Solid-State Single-Molecule Sensing with the Electronic Life-detection Instrument for Enceladus/Europa (ELIE)**

**Authors:** Christopher E. Carr<sup>1,2\*+</sup>, José L. Ramírez-Colón<sup>2+</sup>, Daniel Duzdevich<sup>3-5</sup>, Sam Lee<sup>6</sup>, Masateru Taniguchi<sup>7</sup>, Takahito Ohshiro<sup>7</sup>, Yuki Komoto<sup>7</sup>, Jason M. Soderblom<sup>8</sup>, and M. T. Zuber<sup>8</sup>

#### **Affiliations:**

<sup>1</sup> Daniel Guggenheim School of Aerospace Engineering, Georgia Institute of Technology, Atlanta, GA 30332, USA. <sup>2</sup> School of Earth and Atmospheric Sciences, Georgia Institute of Technology, Atlanta, GA 30332, USA. <sup>3</sup> Massachusetts General Hospital, Department of Molecular Biology, Boston, MA 02114, USA. <sup>4</sup> Howard Hughes Medical Institute, Boston, MA 02114, USA. <sup>5</sup> Current address: Department of Chemistry, University of Chicago, 5735 S Ellis Avenue, Chicago, IL 60637. <sup>6</sup> MIT Department of Electrical Engineering and Computer Science, Cambridge, MA 02139, USA. <sup>7</sup> Osaka University, Institute of Scientific and Industrial Research, Osaka 565-0871 Japan. <sup>8</sup> MIT Department of Earth, Atmospheric and Planetary Sciences, Cambridge, MA 02139, USA.

<sup>+</sup>Co-first authors.

\*Correspondence to: [cecarr@gatech.edu](mailto:cecarr@gatech.edu). Address: ESM Building, Room G10, 620 Cherry St NW, Atlanta, GA 30332, USA

## Table of Contents

<b>Figure S1.</b> Single-molecule conductance and dwell time plots.....	S3
<b>Table S1.</b> Meteorite samples studied.....	S4
<b>Table S2.</b> Environmental samples studied .....	S5
<b>Table S3.</b> Statistical summary of linear regression plots.....	S6
<b>Figure S2.</b> Conductance linear regression plots.....	S7
<b>Figure S3.</b> Dwell time linear regression plots.....	S8
<b>Figure S4.</b> Predicted total event rates of $\alpha$ -amino acids using ELIE.....	S9
<b>Figure S5.</b> Relationship between events dwell time and functional groups of amino acids.....	S10
<b>Figure S6.</b> Abundances of meteoritic and biologically derived $\alpha$ -amino acids .....	S11
<b>Figure S7.</b> Patterns in quantum, redox, and thermodynamic properties of amino acids .....	S12
<b>References</b> .....	S13

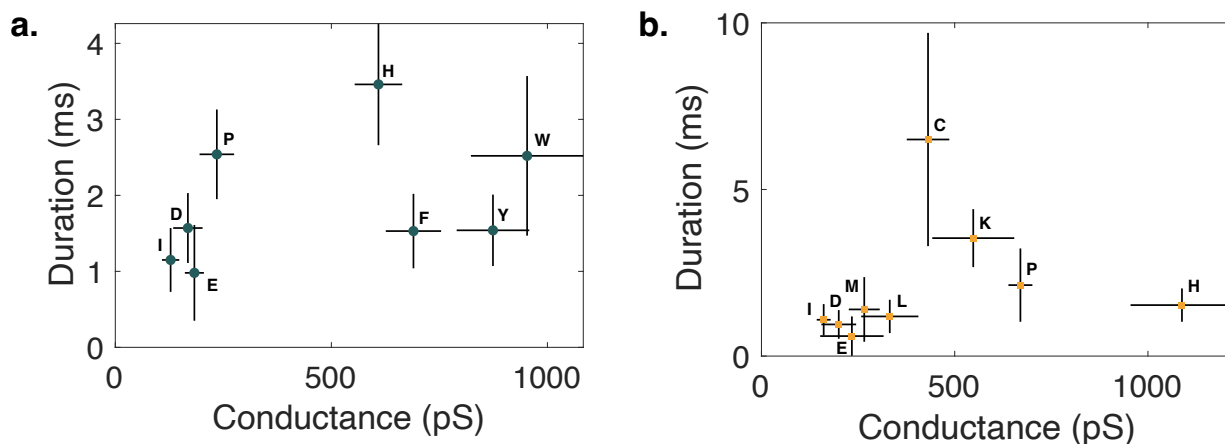


**Figure S1. Two-dimensional plots of single-molecule conductance and duration time for 12 amino acids obtained by Ohshiro *et al.* 2014 using a, 0.7-nm- and b, 0.55-nm-nanogap electrodes. Conductance and duration times denote the peak conductance and peak duration times on their histograms. Error bars were calculated by  $\sigma/N^{0.5}$ , where  $\sigma$  and  $N$  denote the standard deviation and total number of nanogap chips, respectively. Refer to Dataset S1 for the key to the one-letter amino acid designations and conductance and dwell time values.**

**Table S1. Meteorites samples studied with their respective classification.**

Cat.	Meteorite	Class	Amino acids detected <sup>†</sup>	Degree of terrestrial contamination*	Ref.
MGP	Imilac metal	NA	Gly, D/L-Ala, D/L-Asp, D/L-Ser, D-Glu, D/L-Leu, D/L-Ile		[1]
	Imilac silicate	NA	Gly, D/L-Ala, D/L-Asp, D/L-Ser, D/L-Glu, D/L-Leu, D/L-Ile		[1]
Iron meteorites	Canyon Diablo	IAB	Gly, D/L-Ala, D/L-Asp, D/L-Ser, L-Glu, L-Leu, L-Ile	Medium to high	[1]
	Cape York	IIIAB	Gly, D/L-Ala, D/L-Asp, D/L-Ser, D/L-Glu, D/L-Leu, D/L-Ile		[1]
CM meteorites	MET 01070	CM 1	Gly, D/L-Ala, D/L-Asp, D-Val, D/L-Ser, D/L-Glu	Low	[2]
	SCO 06043	CM 1	Gly, D/L-Ala, D/L-Asp, D-Val, D/L-Ser, D/L-Glu		[2]
	Murchison USNM 5453	CM 2	Gly, D/L-Ala, D/L-Asp, D-Val, D/L-Glu		[2]
	LON 94102	CM 2	Gly, D/L-Ala, D/L-Asp, D/L-Ser, D/L-Glu		[2]
	Murchison (Chicago FM)	CM 2	Gly, D/L-Ala, D/L-Asp, D/L-Val, D/L-Ser, D/L-Glu, D/L-Thr	Medium to high	[3]
	Aguas Zarcas UA 2741	CM 2	Gly, D/L-Ala, D/L-Asp, D/L-Val, D/L-Ser, D/L-Glu, D/L-Thr		[3]
	Aguas Zarcas UA 2746	CM 2	Gly, D/L-Ala, D/L-Asp, D/L-Val, D/L-Ser, D/L-Glu, D/L-Thr		[3]
	Paris	CM 2.7	Gly, D/L-Ala, D/L-Asp, D/L-Val, D/L-Glu	Low to medium	[5]
	Asuka 12236	CM 3	Gly, D/L-Ala, D/L-Asp, D/L-Val, D/L-Ser, D/L-Glu	Low to medium	[4]
CR meteorites	GRO 95577	CR 2	Gly, D/L-Ala, D/L-Asp, D/L-Val, D/L-Ser, D/L-Glu	Low	[2]
	MIL 090001	CR 2.4	Gly, D/L-Ala, D/L-Asp, D/L-Val, D/L-Ser, D/L-Glu, D/L-Thr	Low	[6]
	MIL 090657	CR 2.7	Gly, D/L-Ala, D/L-Asp, D/L-Val, D/L-Ser, D/L-Glu, D/L-Thr		[6]
	GRA 95229	CR 2.7	Gly, D/L-Ala, D/L-Asp, D/L-Val, D/L-Ser, D/L-Glu	Low to medium	[7]
	EET 92042	CR 2.8	Gly, D/L-Ala, D/L-Asp, D/L-Val, D/L-Ser, D/L-Glu	Low	[2]
	QUE 99177	CR 2.8	Gly, D/L-Ala, D/L-Asp, D/L-Val, D/L-Ser, D/L-Glu		[2]

**Abbreviations:** Cat. (Category); Ref. (References); NA (Doesn't apply); MET (Meteorite Hills); SCO (Scott Glacier); LON (Lonewolf Nunataks); GRO (Grosvenor Mountains); MIL (Miller Range); GRA (Graves Nunataks); EET (Elephant Moraine); QUE (Queen Alexandra Range).

**Meteorite group key:** MGP (Main Group Pallasites); CR (Renazzo-type chondrites); CM (Mighei-type chondrites).

<sup>†</sup> Refer to Datasets S4, S5, and S6 for the abundances of each enantiomer detected in the meteorite samples.

\* Refer to Figure S8 for more details regarding the degree of terrestrial contamination of the samples.

References: [1] Elsila *et al.* 2021 [2] Glavin *et al.* 2010 [3] Glavin *et al.* 2021 [4] Glavin *et al.* 2020 [5] Martins *et al.* 2015 [6] Aponte *et al.* 2020 [7] Martins *et al.* 2007.



**Table S2. Environmental samples studied with their respective collection site.**

Cat.	Sample ID	Location	Amino acids detected <sup>†</sup>	Degree of biogenic origin*	Ref.
Atacama	ATA03	Salar Laco (margin)	Gly, L-Ala, L-Asp, L-Val, L-Ser, L-Glu, L-Leu, L-Thr, L-Ile, L-Phe	Medium to high	[1]
	ATA05	Laguna Tuyajto (margin)	Gly, L-Ala, L-Asp, L-Val, L-Ser, L-Glu, L-Leu, L-Thr, L-Ile, L-Phe		[1]
	ATA12	Salar Aguas Calientes 3 (margin)	Gly, D/L-Ala, L-Asp, L-Val, L-Ser, D/L-Pro, D/L-Glu, D/L-Leu, D/L-Ile, D/L-Phe		[1]
	ATA15	Salar de Atacama Peine Road (margin)	Gly, D/L-Ala, L-Asp, L-Val, D/L-Pro, L-Glu, D/L-Leu, D/L-Ile, D/L-Phe		[1]
	AT45-A3	Yungay Hill	Gly, D/L-Ala, D/L-Asp, L-Val, D/L-Ser, D/L-Pro, D/L-Glu, D/L-Leu, D/L-Thr, D/L-Ile, D/L-Phe, D/L-Lys, D/L-Tyr	Medium to high	[2]
Antarctica	Wright Valley	Gly, D/L-Ala, D/L-Asp, L-Val, D/L-Ser, D/L-Pro, D/L-Glu, D/L-Leu, D/L-Thr, D/L-Ile, D/L-Phe, D/L-Lys, D/L-Tyr	[2]		
Grassland	Mollisol-1	Hailun, Heilongjian, China	Gly, D/L-Ala, D/L-Asp, L-Val, D/L-Ser, D/L-Pro, D/L-Glu, D/L-Leu, D/L-Thr, D/L-Ile, D/L-Phe, D/L-Lys, D/L-Tyr	High	[3]
Hydrothermal Systems	PC-1	Izena Cauldron	Gly, D/L-Ala, D/L-Asp, L-Val, D/L-Ser, D/L-Glu, D/L-Leu, D/L-Thr, D/L-Ile, D/L-Phe, D/L-Lys	High	[4]
	PC-3	Yoron Cauldron	Gly, D/L-Ala, D/L-Asp, L-Val, D/L-Ser, D/L-Glu, D/L-Leu, D/L-Thr, D/L-Ile, D/L-Phe, D/L-Lys		[4]

Abbreviations: Cat. (Category), Ref. (References).

<sup>†</sup> Refer to Dataset S7 for the abundances of each enantiomer detected in the environmental samples.

\* Refer to Figure S9 for more details regarding the degree of biogenic origin of the amino acids in each sample.

References: [1] Aerts *et al.* 2020 [2] Noell *et al.* 2018 [3] Hou *et al.* 2009 [4] Fuchida *et al.* 2014.

**Table S3. Statistical summary of the linear regression plots.** Fitted by plotting the conductance and dwell time measurements of Ohshiro *et al.* 2014 for 12 amino acids using 0.7-nm- and 0.55-nm-nanogap electrodes against the specific amino acid's molecular weight, volume and HOMO–LUMO gap.

Parameter	Nanogap size	Property	R <sup>2</sup>	Adj. R <sup>2</sup>	p-value
Conductance	0.70 nm	HOMO–LUMO gap	0.971	0.967	7.47 E-6
		Molecular weight	0.827	0.799	0.172 E-2
		Molecular volume	0.846	0.820	0.122 E-2
	0.55 nm	HOMO–LUMO gap	0.110	-0.168 E-1	0.383
		Molecular weight	0.449 E-2	-0.915 E-1	0.584
		Molecular volume	0.729 E-1	-0.595 E-1	0.482
Dwell time	0.70 nm	HOMO–LUMO gap	0.179	0.042	0.297
		Molecular weight	0.362 E-1	-1.244 E-1	0.652
		Molecular volume	0.465 E-1	-0.122	0.608
	0.55 nm	HOMO–LUMO gap	0.262	0.156	0.159
		Molecular weight	0.139	0.017	0.322
		Molecular volume	0.735 E-1	-0.588 E-1	0.480

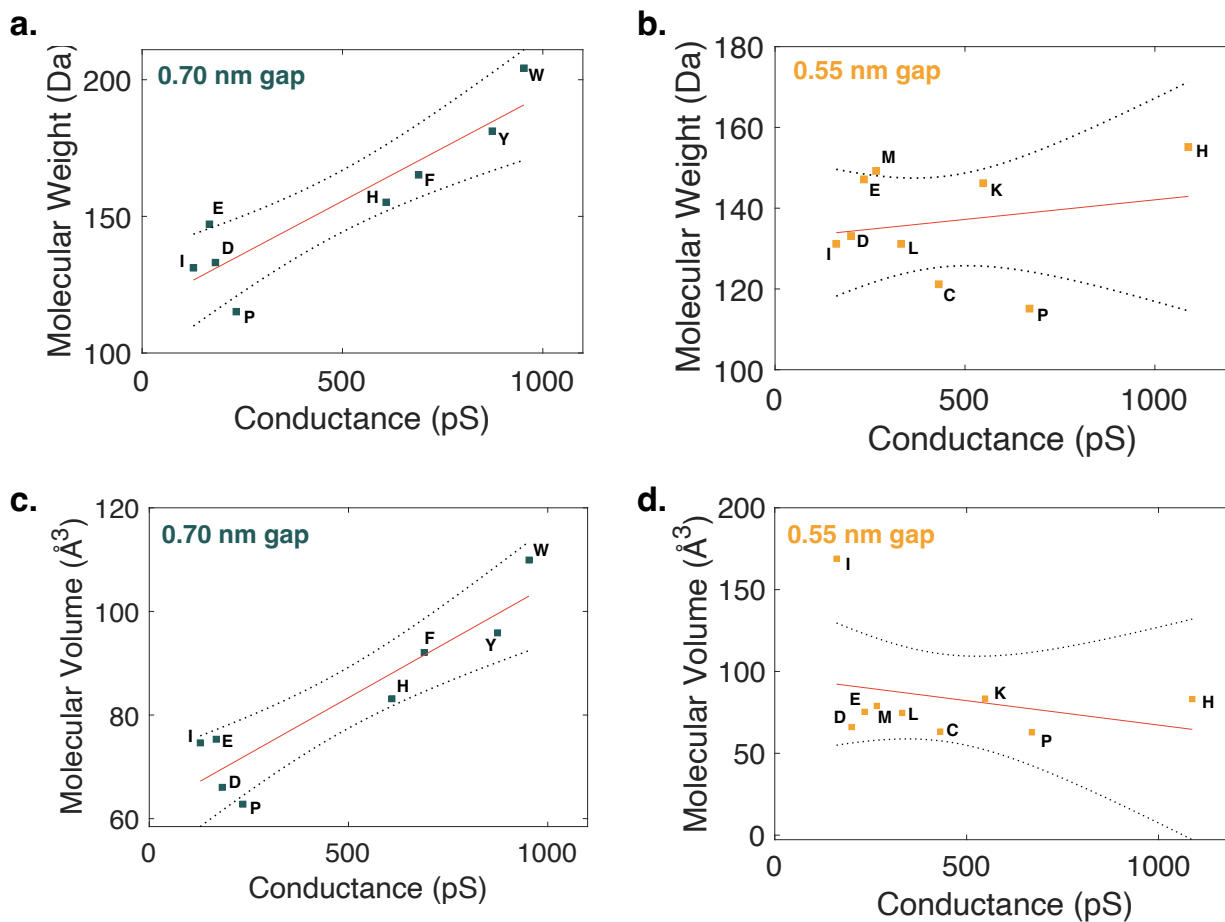


**Figure S2. Linear regression plots of conductance measurements for 12 amino acids obtained by Ohshiro *et al.* 2014 using the a,c, 0.7-nm- and b,d, 0.55-nm-nanogap electrodes against their molecular weight and volume values.**

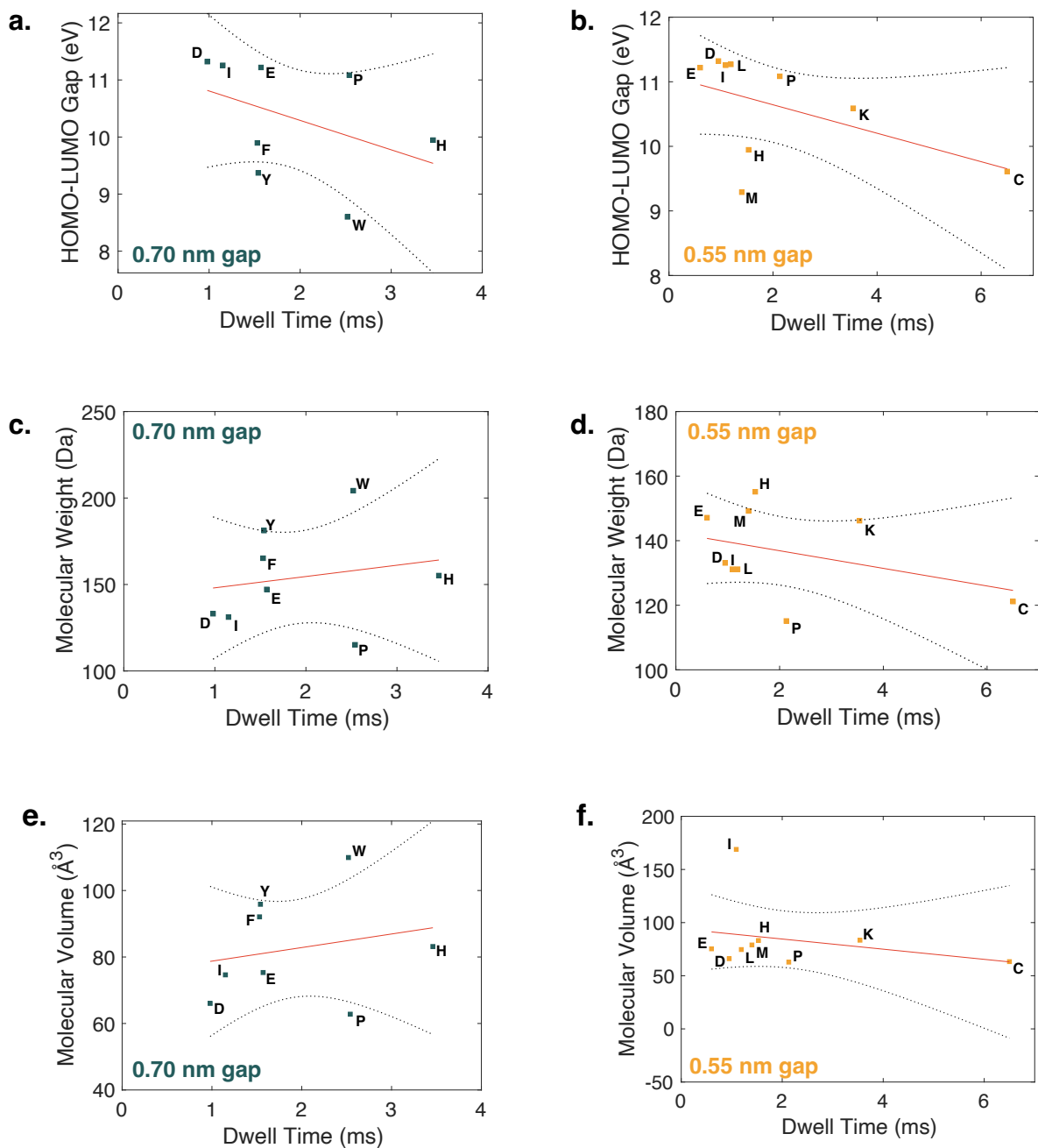


**Figure S3. Linear regression plots of dwell time measurements for 12 amino acids obtained by Ohshiro *et al.* 2014 using the 0.7-nm- (blue dots) and 0.55-nm- (orange dots) nanogap electrodes against their **a,b**, HOMO-LUMO gap (as reported by Granold *et al.* 2018), **c,d**, molecular weight and **e,f**, volume values.**

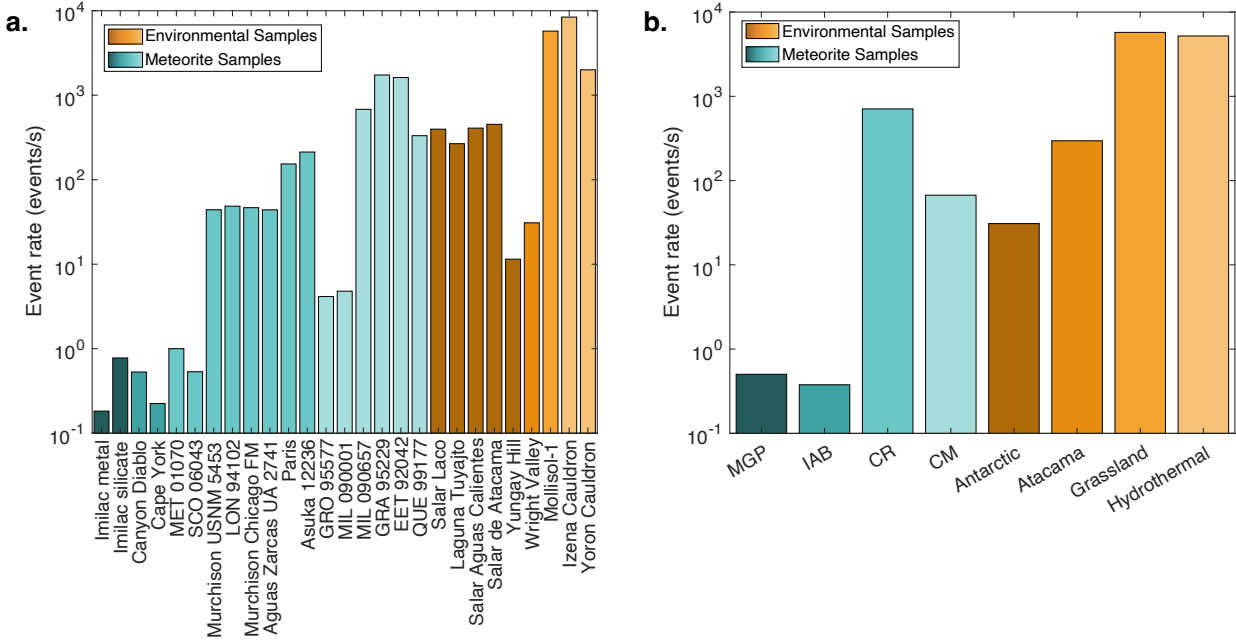


**Figure S4. Predicted total event rates of  $\alpha$ -amino acids derived from biotic and abiotic sources.** Classified by **a**, sample and **b**, category of the meteorite and environmental samples studied (tables S1 and S2). Such predicted events were determined by using an approximate standard event rate observed from the ELIE data of 50 L-proline events/s in 10  $\mu$ M aqueous solutions, and assuming a linear relationship between concentration and event rate.

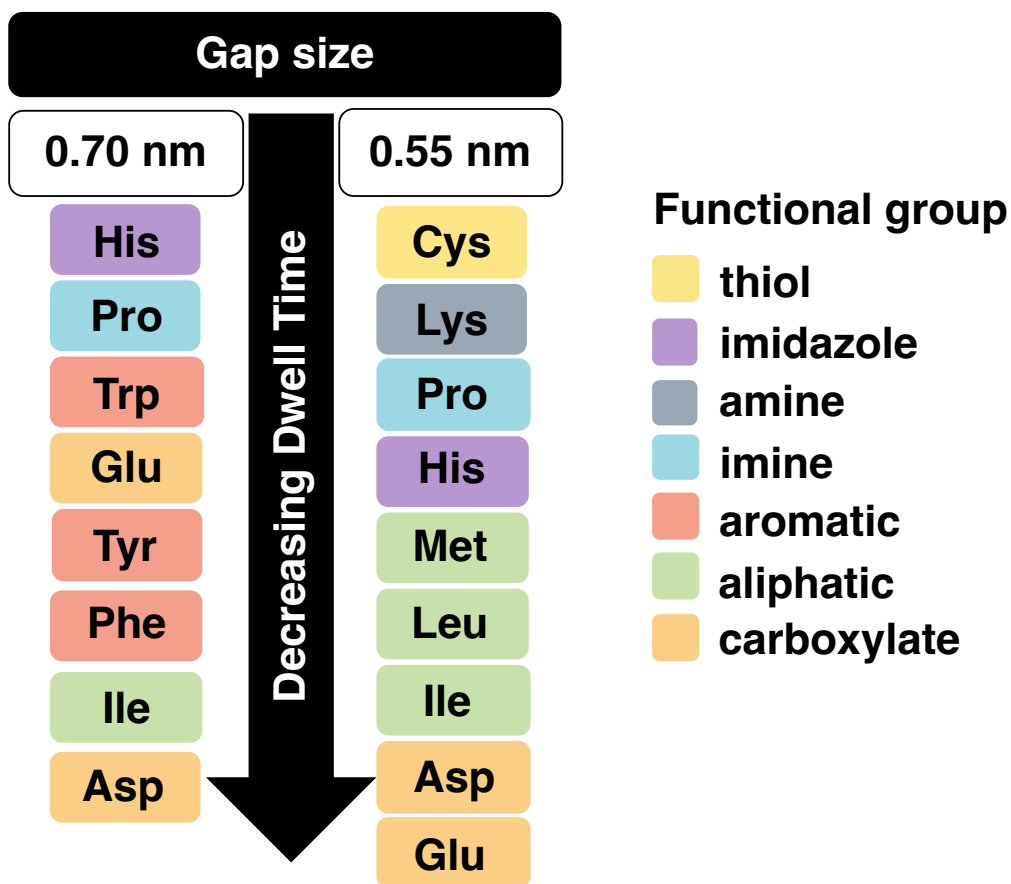


**Figure S5. Dwell time and amino acid functional group correlation.** Relationship between the single-molecule dwell times of the 12 amino acids obtained by Ohshiro *et al.* 2014 using 0.7-nm- and 0.55-nm-nanogap electrodes and their respective functional groups. Refer to Figure 8 for the chemical structure of the functional group pertaining each amino acid.

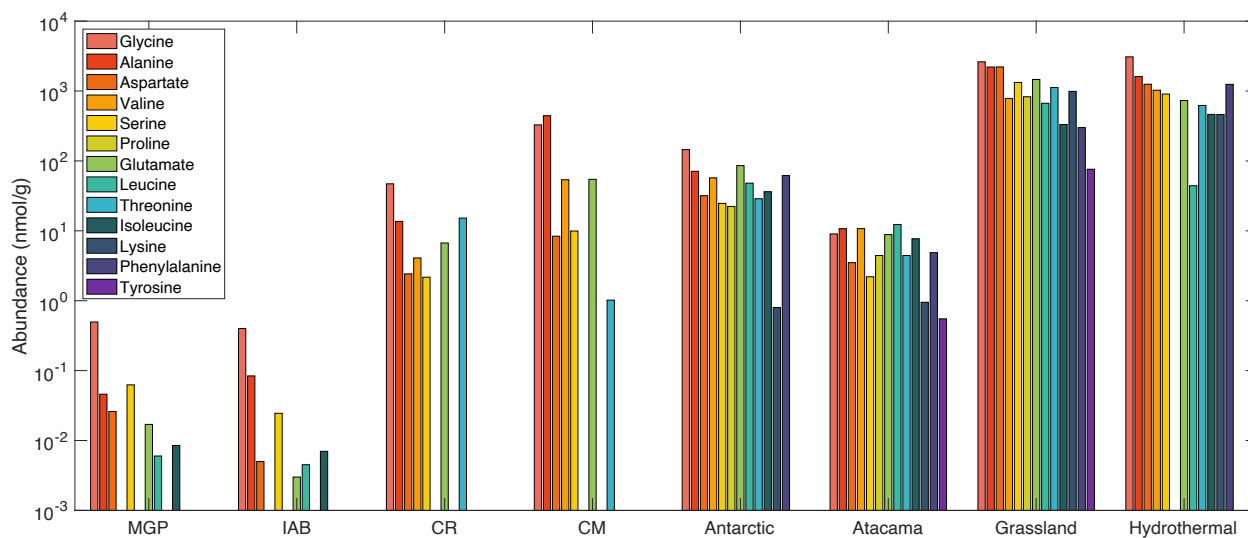


**Figure S6. Distribution patterns of meteoritic  $\alpha$ -amino acids in different meteorite groups and amino acids in various biogenic samples.** Abundance data was averaged following the concentrations reported in tables S1 and S2. The amino acids are placed in the consensus evolutionary order predicted by Trifonov 2009. Meteorite group key: MGP (Main Group Pallasites), IAB (Iron Meteorites Group AB), CR (Renazzo-type chondrites), and CM (Mighei-type chondrites).

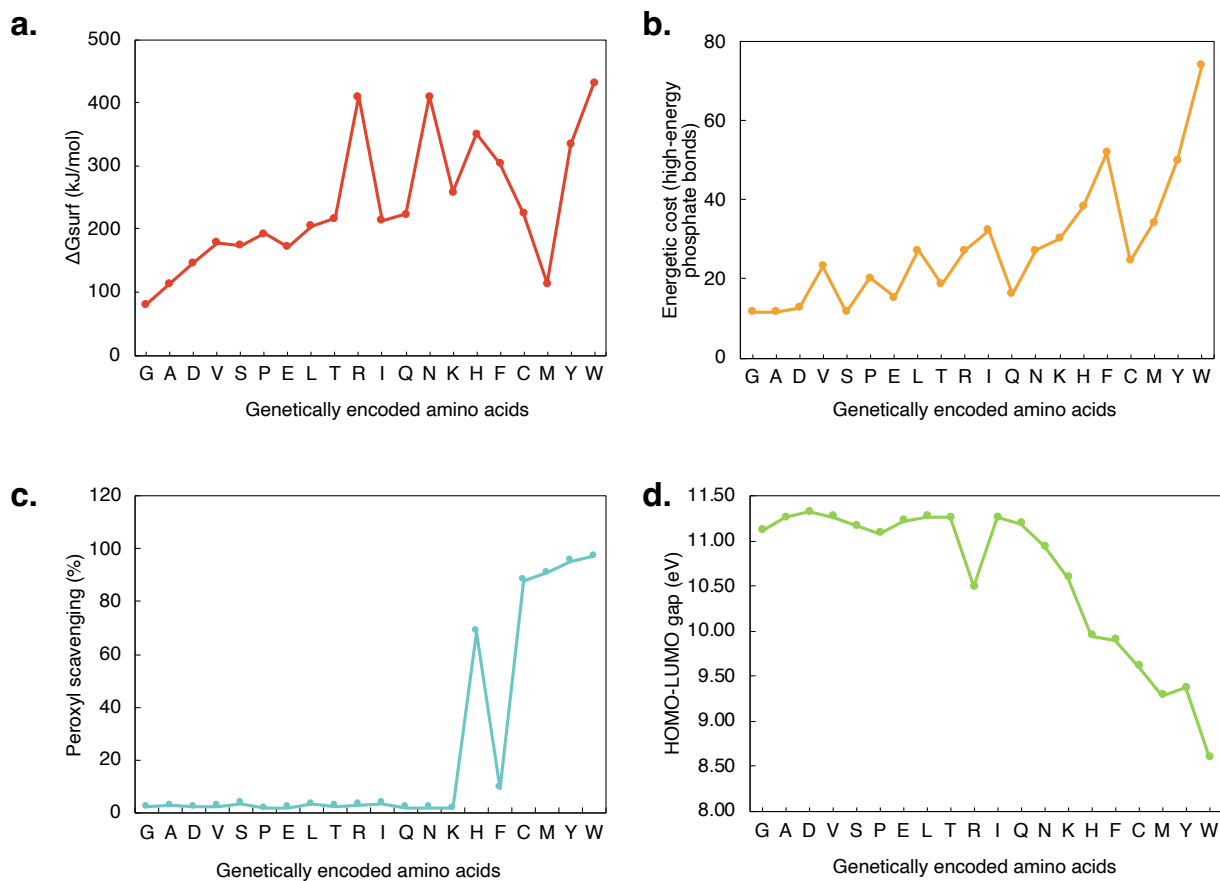


**Figure S7. Patterns of various quantum, redox, and thermodynamic properties of amino acids.** Consensus order of appearance of proteinogenic amino acids within the genetic code, as predicted by Trifonov 2009, in function of their: **a**, Gibbs free energies of net amino acid synthesis reactions in surface seawater (as reported by Amend and Shock 1998); **b**, energetic cost of biosynthesis in *E. coli* and *B. subtilis* (as reported by Akashi and Gojobori 2002); **c**, reactivity towards peroxy radicals and **d**, HOMO-LUMO gap values (as reported by Granold *et al.* 2018). Refer to Dataset 3 for quantitative data regarding each property.



## References

- Aerts J. W., Riedo A., Melton D. J., Martini S., Flahaut J., Meierhenrich U. J., Meinert C., Myrgorodska I., Lindner R., and Ehrenfreund P. (2020) Biosignature Analysis of Mars Soil Analogs from the Atacama Desert: Challenges and Implications for Future Missions to Mars. *Astrobiology*, 20: 766-784.
- Akashi H., and Gojobori T. (2002) Metabolic efficiency and amino acid composition in the proteomes of *Escherichia coli* and *Bacillus subtilis*. *Proceedings of the National Academy of Sciences*, 99: 3695-3700.
- Amend J. P., and Shock E. L. (1998) Energetics of amino acid synthesis in hydrothermal ecosystems. *Science*, 281: 1659-62.
- Aponte J. C., Elsila J. E., Hein J. E., Dworkin J. P., Glavin D. P., McLain H. L., Parker E. T., Cao T., Berger E. L., and Burton A. S. (2020) Analysis of amino acids, hydroxy acids, and amines in CR chondrites. *Meteorit Planet Sci*, 55: 2422-2439.
- Elsila J. E., Johnson N. M., Glavin D. P., Aponte J. C., and Dworkin J. P. (2021) Amino acid abundances and compositions in iron and stony-iron meteorites. *Meteoritics & Planetary Science*, 56: 586-600.
- Fuchida S., Mizuno Y., Masuda H., Toki T., and Makita H. (2014) Concentrations and distributions of amino acids in black and white smoker fluids at temperatures over 200°C. *Organic Geochemistry*, 66: 98-106.
- Glavin D. P., Callahan M. P., Dworkin J. P., and Elsila J. E. (2010) The effects of parent body processes on amino acids in carbonaceous chondrites. *Meteoritics & Planetary Science*, 45: 1948-1972.

- Glavin D. P., Elsila J. E., McLain H. L., Aponte J. C., Parker E. T., Dworkin J. P., Hill D. H., Connolly Jr. H. C., and Lauretta D. S. (2021) Extraterrestrial amino acids and L-enantiomeric excesses in the CM2 carbonaceous chondrites Aguas Zarcas and Murchison. *Meteoritics & Planetary Science*, 56: 148-173.
- Glavin D. P., McLain H. L., Dworkin J. P., Parker E. T., Elsila J. E., Aponte J. C., Simkus D. N., Pozarycki C. I., Graham H. V., Nittler L. R. and others. (2020) Abundant extraterrestrial amino acids in the primitive CM carbonaceous chondrite Asuka 12236. *Meteoritics & Planetary Science*, 55: 1979-2006.
- Granold M., Hajieva P., Tosa M. I., Irimie F. D., and Moosmann B. (2018) Modern diversification of the amino acid repertoire driven by oxygen. *Proc Natl Acad Sci U S A*, 115: 41-46.
- Hou S., He H., Zhang W., Xie H., and Zhang X. (2009) Determination of soil amino acids by high performance liquid chromatography-electro spray ionization-mass spectrometry derivatized with 6-aminoquinolyl-N-hydroxysuccinimidyl carbamate. *Talanta*, 80: 440-7.
- Martins Z., Alexander C. M. O. D., Orzechowska G. E., Fogel M. L., and Ehrenfreund P. (2007) Indigenous amino acids in primitive CR meteorites. *Meteoritics & Planetary Science*, 42: 2125-2136.
- Martins Z., Modica P., Zanda B., and d'Hendecourt L. L. S. (2015) The amino acid and hydrocarbon contents of the Paris meteorite: Insights into the most primitive CM chondrite. *Meteoritics & Planetary Science*, 50: 926-943.
- Noell A. C., Fisher A. M., Fors-Francis K., and Sherrit S. (2018) Subcritical water extraction of amino acids from Mars analog soils. *Electrophoresis*, 39: 2854-2863.

Ohshiro T., Tsutsui M., Yokota K., Furuhashi M., Taniguchi M., and Kawai T. (2014) Detection of post-translational modifications in single peptides using electron tunnelling currents.

In: *Nat Nano*, Nature Publishing Group, pp 835.

Trifonov E. N. (2009) The origin of the genetic code and of the earliest oligopeptides. *Res*

*Microbiol*, 160: 481-6.

**Dataset S1. Single-molecule conductance and duration time for 13 amino acid molecules using 0.7-nm- and 0.55-nm-nanogap electrodes.**

Amino Acid	Abbreviation	Symbol	Gap_nm	Conductance_pS	Spread_pS	Dwell_time_ms	Spread_ms
Aspartic Acid	Asp	D	0.7	183	22	0.98	0.63
Isoleucine	Ile	I	0.7	128	20	1.15	0.42
Glutamic Acid	Glu	E	0.7	168	34	1.57	0.46
Proline	Pro	P	0.7	235	40	2.54	0.59
Histidine	His	H	0.7	609	55	3.46	0.8
Phenylalanine	Phe	F	0.7	690	64	1.53	0.49
Tyrosine	Tyr	Y	0.7	874	84	1.54	0.47
Tryptophan	Trp	W	0.7	953	130	2.52	1.05
Aspartic Acid	Asp	D	0.55	200	45	0.95	0.43
Isoleucine	Ile	I	0.55	161	18	1.09	0.47
Glutamic Acid	Glu	E	0.55	234	82	0.6	0.59
Proline	Pro	P	0.55	670	31	2.13	1.1
Histidine	His	H	0.55	1088	133	1.53	0.5
Lysine	Lys	K	0.55	548	106	3.54	0.87
Cysteine	Cys	C	0.55	431	55	6.5	3.2
Methionine	Met	M	0.55	266	40	1.4	1.0
Leucine	Leu	L	0.55	332	74	1.2	0.5

**Data obtained from the following work:**

Ohshiro T., Tsutsui M., Yokota K., Furuhashi M., Taniguchi M., and Kawai T. (2014)

Detection of post-translational modifications in single peptides using electron tunnelling currents. In: *Nat Nano, Nature Publishing Group*, pp 835.

**Dataset S2. HOMO–LUMO gaps of 62 Murchison meteorite AAs, 21 genetically encoded AAs, and various metabolic descendants of the shikimate pathway calculated using semiempirical methods (AM1).**

Name	HOMO–LUMO gap	Category
2,3-Diaminobutanoic acid	11.02	0.00
2,3-Diaminopropanoic acid	10.90	0.00
2,4-Diaminobutanoic acid	10.83	0.00
2-Amino-2,3,3-trimethylbutanoic acid	11.20	0.00
2-Amino-2,3-dimethylbutanoic acid	11.22	0.00
2-Amino-2,3-dimethylpentanoic acid	11.17	0.00
2-Amino-2,4-dimethylpentanoic acid	11.40	0.00
2-Amino-2-ethyl-3-methylbutanoic acid	11.30	0.00
2-Amino-2-ethylbutanoic acid	11.28	0.00
2-Amino-2-ethylpentanoic acid	11.25	0.00
2-Amino-2-methylhexanoic acid	11.34	0.00
2-Amino-3,3-dimethylpentanoic acid	11.23	0.00
2-Amino-3,4-dimethylpentanoic acid	11.21	0.00
2-Amino-3-ethylpentanoic acid	11.17	0.00
2-Amino-3-methylhexanoic acid	11.23	0.00
2-Amino-4,4-dimethylpentanoic acid	11.24	0.00
2-Amino-4-methylhexanoic acid	11.21	0.00
2-Amino-5-methylhexanoic acid	11.24	0.00
2-Aminoheptanoic acid	11.24	0.00
2-Methylaspartic acid	11.47	0.00
2-Methylglutamic acid	11.40	0.00
2-Methyl-norvaline	11.30	0.00
3,3'-Diaminoisobutanoic acid	10.65	0.00
3-Amino-2,2-dimethylpropanoic acid	11.04	0.00
3-Amino-2-ethylpropanoic acid	10.98	0.00
3-Amino-2-methylbutanoic acid	11.02	0.00
3-Amino-3-methylbutanoic acid	10.84	0.00
3-Aminopentanoic acid	11.00	0.00
3-Methylaspartic acid	11.32	0.00
4,4'-Diaminoisopentanoic acid	10.87	0.00
4-Amino-2-methylbutanoic acid	10.95	0.00
4-Amino-3-methylbutanoic acid	10.80	0.00
4-Aminopentanoic acid	10.89	0.00
5-Aminopentanoic acid	10.74	0.00
Alanine	11.26	0.00
Alpha-aminoadipic acid	11.26	0.00
Alpha-aminobutyric acid	11.23	0.00
Alpha-aminoisobutyric acid	11.42	0.00
Alpha-aminopimelic acid	11.24	0.00
Alpha-methyl norleucine	11.30	0.00
Alpha-methyl valine	11.38	0.00
Aspartic acid	11.32	0.00
Beta-alanine	11.26	0.00
Beta-aminobutyric acid	11.00	0.00
Beta-aminoisobutyric acid	10.91	0.00
Cycloleucine	11.34	0.00
Gamma-aminobutyric acid	10.90	0.00
Glutamic acid	11.22	0.00
Glycine	11.11	0.00
Isoleucine	11.26	0.00
Isovaline	11.27	0.00
Leucine	11.27	0.00
N-ethylglycine	10.64	0.00
N-methylalanine	10.85	0.00
Norleucine	11.31	0.00
Norvaline	11.26	0.00
Ornithine	10.83	0.00
Pipecolic acid	10.76	0.00
Proline	11.09	0.00
Pseudoleucine	11.21	0.00
Sarcosine	10.67	0.00
Valine	11.27	0.00
Glycine (G)	11.11	1.00
Alanine (A)	11.26	1.00
Aspartate (D)	11.32	1.00
Valine (V)	11.27	1.00
Serine (S)	11.17	1.00
Proline (P)	11.09	1.00
Glutamate (E)	11.22	1.00
Leucine (L)	11.27	1.00
Threonine (T)	11.26	1.00
Arginine (R)	10.49	1.00
Isoleucine (I)	11.26	1.00
Glutamine (Q)	11.19	1.00
Asparagine (N)	10.94	1.00
Lysine (K)	10.59	1.00
Histidine (H)	9.95	1.00
Phenylalanine (F)	9.90	1.00
Cysteine (C)	9.61	1.00
Methionine (M)	9.29	1.00
Tyrosine (Y)	9.37	1.00
Tryptophan (W)	8.60	1.00
Selenocysteine (U)	7.67	1.00
Coumaryl alcohol	8.51	2.00
CTC	8.62	2.00
CTQ	7.49	2.00
Indolyloquinol	7.96	2.00
LTQ	7.78	2.00
Melatonin	8.46	2.00
Plastoquinol	8.70	2.00
PQQ	7.96	2.00
Quercetin	7.75	2.00
Resveratrol	7.85	2.00
Tocopherol	8.69	2.00
Tocotrienol	8.69	2.00
TPQ	8.47	2.00
TTQ	7.15	2.00
Ubiquinol	8.58	2.00

Legend
0 = Meteoritic amino acid
1 = Proteinogenic amino acid
2 = Metabolic descendants of shikimate pathway

**Data provided by the authors of the following work:**

Granold M., Hajieva P., Tosa M. I., Irimie F. D., and Moosmann B. (2018) Modern diversification of the amino acid repertoire driven by oxygen. *Proc Natl Acad Sci USA*, 115: 41-46.

Dataset S3. Quantitative data of studied quantum, redox, and thermodynamic properties of amino acids.

Amino Acid	Symbol	Mass (Da)	Volume (Å <sup>3</sup> )	HOMO–LUMO gap (eV)	ΔG <sub>surf</sub> (kJ/mol)	ΔG <sub>hydro</sub> (kJ/mol)	Energetic cost (phosphate bond)	peroxyl radical scavenging (%)
Glycine	G	75.07	43.095	11.11	80.49	14.89	11.7	2.305401829
Alanine	A	89.09	51.446	11.26	113.66	-12.12	11.7	2.682072313
Aspartic Acid	D	133.1	66.042	11.32	146.74	32.78	12.7	2.290156113
Valine	V	117.15	66.618	11.27	178	-70.12	23.3	2.462530897
Serine	S	105.09	55.144	11.17	173.73	69.47	11.7	3.516056518
Proline	P	115.13	62.793	11.09	192.83	-38.75	20.3	1.621778013
Glutamic Acid	E	147.13	75.329	11.22	172.13	-1.43	15.3	1.909034124
Leucine	L	131.17	74.658	11.27	205.03	-105.53	27.3	3.30172054
Threonine	T	119.12	62.285	11.26	216.5	53.51	18.7	2.365935841
Arginine	R	174.2	97.202	10.49	409.46	197.52	27.3	3.005027498
Isoleucine	I	131.17	74.627	11.26	213.93	-96.4	32.3	3.616060079
Glutamine	Q	146.14	78.125	11.19	223.36	44.03	16.3	1.956582568
Asparagine	N	132.12	68.811	10.94	409.46	83.53	27.3	2.012513673
Lysine	K	146.19	83.417	10.59	258.56	-28.33	30.3	1.703616558
Histidine	H	155.15	83.147	9.95	350.52	154.48	38.3	68.49616863
Phenylalanine	F	165.19	92.076	9.90	303.64	-114.54	52	9.258049656
Cysteine	C	121.16	63.274	9.61	224.67	60.24	24.7	87.79348992
Methionine	M	149.21	78.962	9.29	113.22	-174.71	34.3	90.89376334
Tyrosine	Y	181.19	95.863	9.37	334.2	-59.53	50	95.13122137
Tryptophan	W	204.23	109.919	8.60	431.17	-38.99	74.3	97.0868436

Reported values in the following references:

**Gibbs free energy of net amino acid synthesis reactions in surface seawater:** Amend J. P., and Shock E. L. (1998) Energetics of amino acid synthesis in hydrothermal ecosystems. *Science*, 281: 1659-62.

**Energetic cost:** Akashi H., and Gojobori T. (2002) Metabolic efficiency and amino acid composition in the proteomes of *Escherichia coli* and *Bacillus subtilis*. *Proceedings of the National Academy of Sciences*, 99: 3695-3700.

**HOMO–LUMO gaps and reactivity towards peroxyl radicals:** Granold M., Hajieva P., Tosa M. I., Irimie F. D., and Moosmann B. (2018) Modern diversification of the amino acid repertoire driven by oxygen. *Proc Natl Acad Sci USA*, 115: 41-46.

**Figure S8. Methods employed in the extraction of amino acids from meteorites studied, along the degree of terrestrial contamination of the samples.**

Ref.	Methods	Extent of Terrestrial Contamination of $\alpha$ -AAs
Aponte et al. 2020	<p><b>Extraction:</b> Hot water extraction at 100 °C for 24 h. Half of the samples were acid-vapor hydrolyzed (6M HCl) for 3 h at 150 °C.</p> <p><b>Purification:</b> Purification via cation-exchange chromatography (with norleucine as internal standard). Amino acids eluted with 2 M NH<sub>4</sub>OH.</p> <p><b>Derivatization and separation:</b> Derivatization with OPA/NAC. OPA/NAC amino acid derivatives were further analyzed with a UPLC-FD/ToF-MS.</p>	<p><b>LOW</b></p> <p>Most protein amino acids present had <b>D/L ratios</b> nearly equal to 1. <b>L-valine</b> abundance (in <b>MIL 090657</b>) showed to be the only exception; showing a lower D/L ratio and being attributed to terrestrial contamination.</p> <p>Deuterium compositions of the samples reveal values ranging from +975 to +5,797; biological samples commonly show values between +50 and -370.</p>
Martins et al. 2007	<p><b>Extraction:</b> Hot water extraction at 100 °C for 24 h. Half of the samples were dried under vacuum and acid-vapor hydrolyzed (6M HCl) for 3 h at 150 °C.</p> <p><b>Purification:</b> Purification via cation-exchange chromatography. Amino acids eluted with NH<sub>4</sub>OH and dried under vacuum. Residues redissolved in 100 <math>\mu</math>L of water.</p> <p><b>Derivatization and separation:</b> Samples were buffered with 0.1 M sodium borate and derivatized with OPA/NAC and TFAA/isopropanol. OPA/NAC and TFAA/isopropanol amino acid derivatives were further analyzed with a HPLC-FD and a GC-MS, respectively.</p>	<p><b>MEDIUM TO LOW</b></p> <p>Both protein and non-protein amino acids present were nearly <b>racemical</b>. <b>Glutamic acid</b> abundance (in <b>EET92042</b> and <b>GRA95229</b>) showed to be the only exception; showing a lower D/L ratio and being attributed to terrestrial contamination, specifically during the curation process. <b>GRO95577</b> showed significant terrestrial contamination with all amino acids D/L ratios smaller than <b>0.8</b>.</p> <p><b><math>\delta^{13}C</math> values</b> of <math>\alpha</math>-amino acids present in the EET92042 and GRA95229 meteorites were clearly outside the terrestrial range. <b>L-glutamic acid</b> values showed to also be smaller (like D/L ratios) and within the range of the terrestrial range; However, is still unclear how terrestrial contamination preferentially impacted just glutamic acid abundances.</p>
Martins et al. 2015	<p><b>Extraction:</b> Hot water extraction at 100 °C for 24 h. Half of the water supernatants were dried under vacuum and acid-vapor hydrolyzed (6M HCl) for 3 h at 150 °C.</p> <p><b>Purification:</b> Purification via cation-exchange chromatography. Amino acids eluted with NH<sub>4</sub>OH and dried under vacuum.</p> <p><b>Derivatization and separation:</b> Samples were derivatized with OPA/NAC and TFAA/IPA. TFAA/IPA amino acid derivatives were further analyzed with a GC-MS.</p>	<p><b>MEDIUM TO LOW</b></p> <p>The D/L values were found to range from 0.72 to 0.99, indicating a certain degree of terrestrial contamination, mainly due to the handling history of this meteorite.</p>
Glavin et al. 2010		<p><b>LOW</b></p> <p>Enantiomeric ratios measured from protein amino acids were mostly found to be racemic (<b>0.9-1.0</b>), even for the high abundance of <b><math>\alpha</math>-alanine</b> in the <b>EET 92042</b> sample (Predicted that the parent body had high abundances of the precursor for alpha alanine). Exception is seen with <b>aspartic and glutamic acid</b> in the <b>USNM 5453</b> sample (D/L ratios of 0.67 and 0.61).</p>
Glavin et al. 2020	<p><b>Extraction:</b> Hot water extraction at 100 °C for 24 h. Half of the samples were acid-vapor hydrolyzed (6M HCl) for 3 h at 150 °C.</p> <p><b>Purification:</b> Purification via cation-exchange chromatography (with norleucine as internal standard). Amino acids eluted with 2 M NH<sub>4</sub>OH and dried in vacuum. Samples were redissolved in 100 <math>\mu</math>L of water.</p> <p><b>Derivatization and separation:</b> Derivatization with OPA/NAC. OPA/NAC amino acid derivatives were further analyzed with a UPLC-FD/ToF-MS.</p>	<p><b>MEDIUM TO LOW</b></p> <p>L-excesses were observed for <b>serine, glutamic acid and aspartic acid</b> in the <b>A-12236</b> extracts. Increases in the abundances of these three protein amino acids were also seen after <b>acid hydrolysis</b> (which is usually accounted to terrestrial contamination). However, deficiency of this increase in <b>alanine and glycine</b> (which abundances are typically the same or higher to these three amino acids in proteins) after acid hydrolysis, poses an inconsistent trend.</p>
Glavin et al. 2021		<p><b>MEDIUM TO HIGH</b></p> <p>Elevated abundances of protein amino acids in the Aguas Zarcas meteorite UA 2746 compared to the 2741 sample are consistent with both some terrestrial amino acid exposure of the Aguas Zarcas meteorites after their fall and visual observations of plant material in UA 2746.</p> <p>The similar <math>\delta^{13}C</math> values obtained for D-L- alanine, glutamic acid, and aspartic acid in the UA 2746 meteorite when compared to the Aguas Zarcas soil provide substantial evidence for terrestrial contamination. Also, lower values of L-alanine and L-glutamic acid in UA 2746 than their respective D-enantiomers further imply terrestrial contamination of this meteorite sample.</p>
Elsila et al. 2021	<p><b>Meteorite Processing:</b> Samples were initially sonicated in water, then processed into powder using a cryogenic ball mill and furtherly grinded using stainless steel grinding balls.</p> <p><b>Extraction:</b> Hot water extraction at 100 °C for 24 h. Half of the samples were acid-vapor hydrolyzed (6M HCl) for 3 h at 150 °C.</p> <p><b>Purification:</b> Purification of hydrolyzed and unhydrolyzed samples via cation-exchange chromatography. Amino acids eluted with 2 M NH<sub>4</sub>OH.</p> <p><b>Derivatization and separation:</b> Derivatization with OPA/NAC. OPA/NAC amino acid derivatives were further analyzed with a LC-FD/ToF-MS.</p>	<p><b>MEDIUM TO HIGH</b></p> <p>Terrestrial contamination of the meteorite samples seems apparent due to increased excesses of proteinogenic amino acids in the <b>water washes controls</b> of the meteorite pieces during the meteorite processing in comparison to those controls from the interior of the cryogenic mill. Contamination of the meteorites is attributed to years spent in <b>terrestrial environments and curation</b>.</p>

**References:**

- Aponte J. C., Elsila J. E., Hein J. E., Dworkin J. P., Glavin D. P., McLain H. L., Parker E. T., Cao T., Berger E. L., and Burton A. S. (2020) Analysis of amino acids, hydroxy acids, and amines in CR chondrites. *Meteoritics & Planetary Science*, 55: 2422-2439.
- Martins Z., Alexander C. M. O.D., Orzechowska G. E., Fogel M. L., and Ehrenfreund P. (2007) Indigenous amino acids in primitive CR meteorites. *Meteoritics & Planetary Science*, 42: 2125-2136.
- Martins Z., Modica P., Zanda B., and d'Hendecourt L. S. (2015) The amino acid and hydrocarbon contents of the Paris meteorite: Insights into the most primitive CM chondrite. *Meteoritics & Planetary Science*, 50: 926-943.
- Glavin D. P., Callahan M. P., Dworkin J. P., and Elsila J. E. (2010) The effects of parent body processes on amino acids in carbonaceous chondrites. *Meteoritics & Planetary Science*, 45: 1948-1972.
- Glavin D. P., Elsila J. E., McLain H. L., Aponte J. C., Parker E. T., Dworkin J. P., Hill D. H., Connolly Jr. H. C., and Lauretta D. S. (2021) Extraterrestrial amino acids and L-enantiomeric excesses in the CM2 carbonaceous chondrites Aguas Zarcas and Murchison. *Meteoritics & Planetary Science*, 56: 148-173.
- Glavin D. P., McLain H. L., Dworkin J. P., Parker E. T., Elsila J. E., Aponte J. C., Simkus D. N., Pozarycki C. I., Graham H. V., Nittler L. R., and others. (2020) Abundant extraterrestrial amino acids in the primitive CM carbonaceous chondrite Asuka 12236. *Meteoritics & Planetary Science*, 55: 1979-2006.
- Elsila J. E., Johnson N. M., Glavin D. P., Aponte J. C., and Dworkin J. P. (2021) Amino acid abundances and compositions in iron and stony-iron meteorites. *Meteoritics & Planetary Science*, 56: 586-600.

**Dataset S4. Amino acid abundances (nmol/g) in meteorites samples of the Main Group Pallasites and Iron meteorites group AB.**

Amino acid	MGP				IAB			
	Elsila et al. 2021 (nmol/g)							
	Imilac metal	SD	Imilac silicate	SD	Canyon Diablo	SD	Cape York	SD
D-aspartic acid	0.0013	SM	0.0062	SM	Below limit	NA	0.0019	SM
L-aspartic acid	Below limit	NA	0.0446	SM	0.0035	0	0.0045	SM
D-glutamic acid	Below limit	NA	0.0016	SM	Not detected	NA	Below limit	SM
L-glutamic acid	Not detected	NA	0.0156	SM	0.0052	0	0.0013	SM
D-serine	0.002	SM	0.0146	SM	0.0017	0	0.0015	SM
L-serine	0.0035	SM	0.1044	SM	0.0387	0	0.0078	SM
glycine	0.1902	SM	0.8024	SM	0.5274	0.06	0.2728	SM
D-alanine	0.0069	SM	0.0164	SM	0.0208	0	0.0078	SM
L-alanine	0.0107	SM	0.0573	SM	0.1238	0.02	0.015	SM
D-isoleucine	Below limit	NA	Below limit	NA	Not detected	NA	Below limit	NA
L-isoleucine	0.0018	SM	0.0149	SM	0.0131	0	0.0014	SM
D-leucine	Below limit	NA	Below limit	NA	Not detected	NA	Below limit	NA
L-leucine	0.0016	SM	0.0096	SM	0.0081	0	0.0009	SM

SM: Single Measurement

NA: Doesn't apply



Dataset S5. Amino acid abundances (nmol/g) in meteorites samples of the Mighei-type chondrites group.

Amino acid	Abundance (nmol/g)																
	Glavin et al. 2010								Glavin et al. 2020				Martins et al. 2015				
	MET 01070	SD	SCO 06043	SD	Murchison USNM 5453	SD	LON 94102	SD	Asuka 12236	SD	Murchison (Chicago Field Museum)	SD	Agua Zarcas UA 2741	SD	Paris	SD	
D-aspartic acid	< 0.01	NA	< 0.01	NA	1.42	0.11	0.89	0.47	2.4	0.1	0.59	0.02	0.16	0.06	1.01	0.04	
L-aspartic acid	< 0.02	NA	< 0.02	NA	2.11	0.17	0.84	0.31	4.9	0.2	3	0.1	0.5	0.2	1.5	0.04	
D-glutamic acid	< 0.02	NA	< 0.01	NA	3.78	0.62	4.02	1.45	3.1	0.2	1.03	0.03	0.59	0.01	5.6	0.4	
L-glutamic acid	< 0.02	NA	< 0.02	NA	6.16	0.85	4.15	1.44	8.4	0.5	6.3	0.1	3.7	0.1	6.7	0.5	
D-serine	< 0.01	NA	< 0.02	NA	NR	NA	0.74	0.52	1.1	0.2	0.13	0.03	0.3	0.2	NR	NA	
L-serine	< 0.02	NA	< 0.02	NA	NR	NA	0.69	0.23	5.0	0.2	3.5	0.1	1.5	0.9	NR	NA	
D-threonine	NR	NA	NR	NA	NR	NA	NR	NA	ID	NA	0.02	0.01	0.2	0.2	NR	NA	
L-threonine	NR	NA	NR	NA	NR	NA	NR	NA	ID	NA	2.21	0.05	28	1	NR	NA	
glycine	0.79	0.11	0.36	0.08	19.59	5.39	25.50	7.74	160.0	5	40	3	20	3	110	5	
D-alanine	0.14	0.02	0.08	0.01	4.45	0.74	6.19	2.22	28.0	2	2.2	0.1	1.6	0.1	8	0.4	
L-alanine	0.16	0.02	0.08	0.02	5.40	1.2	5.60	2.15	30.0	2	3	0.2	3.5	0.4	10.8	0.5	
D-valine	< 0.01	NA	0.02	0.01	1.20	0.04	NR	NA	5.6	0.9	0.55	0.02	0.35	0.03	4.9	0.1	
L-valine	ABL	NA	ABL	NA	ABL	NA	NR	NA	6.8	0.4	2.8	0.1	1.2	0.1	5.2	0.2	

NA: Doesn't apply
NR: Not reported
ABL: Above blank level
ID: Interfering detection

**Dataset S6. Amino acid abundances (nmol/g) in meteorite samples of the Renazzo-type chondrites group.**

Amino acid	Abundance (nmol/g)											
	Aponte et al. 2020		Martins et al. 2007		Glavin et al. 2010						Aponte et al. 2020	
	MIL 090657	SD	GRA 95229	SD	EET 92042	SD	QUE 99177	SD	GRO 95577	SD	MIL 090001	SD
D-aspartic acid	8.18	2.66	5.02	0.05	7.72	1.18	4.1	1.61	< 0.06	NA	0.19	0.01
L-aspartic acid	7.9	2.09	5.23	0.07	7.63	1.09	4.03	1.28	< 0.02	NA	0.18	0.05
D-glutamic acid	50	11.2	20.4	0.6	68.6	13.4	23.9	4.1	< 0.06	NA	0.31	0.11
L-glutamic acid	46.3	4.3	24.9	2.2	69.2	11.9	23.4	3.7	< 0.01	NA	0.25	0.04
D-serine	3.24	0.37	17.2	0.8	2.46	13.5	6.52	4.05	< 0.04	NA	0.05	0.01
L-serine	2.62	0.32			21.6	11.8	5.79	3.61	<0.03	NA	0.06	0.01
D-threonine	1.11	0.18	NR	NA	NR	NA	NR	NA	NR	NA	< 0.01	NA
L-threonine	0.91	0.17	NR	NA	NR	NA	NR	NA	NR	NA	< 0.01	NA
D-alanine	260	18	569	5	450	104	40.3	5.11	0.52	0.18	0.93	0.23
L-alanine	267	20	569	32	464	84	39.8	6.7	0.39	0.06	1.06	0.3
glycine	275	23	770	5	726	205	188	45	3.7	1	3.46	0.88
D-valine	13.6	3.3	49.8	1.8	61.6	3.6	29.4	1.8	0.05	0.01	0.06	0.01
L-valine	17.9	1.4	51.7	1.3	65.3	4.3	33	1.2	0.1	0.01	0.14	0.02

NA: Doesn't apply

NR: Not reported

Figure S9. Methods employed in the extraction of amino acids from environmental samples studied, along the presence of protein  $\alpha$ -AAs on each.

Ref.	Methods	Presence of protein $\alpha$ -AAs in samples
Aerts et al. 2020	<b>Extraction:</b> Hot water extraction in 3 mL at 100 °C for 24 h. Then, centrifugation at 2500 rpm for 10 min. Samples were dried. Half of the samples were acid-vapor hydrolyzed (6M HCl) for 3 h at 150 °C.	<b>MEDIUM TO HIGH</b>
	<b>Purification:</b> Purification via cation-exchange resin with washes of basic-neutral-acid-basic solutions. Amino acids eluted with 2 M NH <sub>4</sub> OH. Ammonia was removed through drying.	Most protein amino acids present in samples analyzed via GC-MS (were both D- and L- enantiomeric abundances were determined) had <b>D/L ratios</b> below <b>0.25</b> ; highly indicative of a biotic origin. Most amino acids were present in a similar order of magnitude; also indicative of biotic origin of these molecules. Microbial communities (a total of 1404 OTU's) were identified in all samples from the four different regions analyzed.
	<b>Derivatization and separation:</b> Derivatization with OPANAC and ECHFBE. OPANAC amino acid derivatives were further analyzed with a LC-MS. ECHFBE amino acid derivatives were further analyzed with a GC-MS.	
<hr/>		
Noell et al. 2018	<b>Extraction:</b> Soil samples were acid-vapor hydrolyzed (6 N HCl) for 15 min at 160 °C.	<b>MEDIUM TO HIGH</b>
	<b>Purification:</b> Purification via cation-exchange resin with washes of basic-neutral-acid-basic solutions. Amino acids eluted with NH <sub>4</sub> OH under basic conditions and lyophilized.	Protein amino acids of major abundances included <b>Gly, Val, Glu, Ala, and Leu</b> , and presneted abundances similar in magnitude (indicative of biotic origin).
	<b>Derivatization and separation:</b> Samples were derivatized with AccQ-Tag fluorescent reagent and further analyzed via HPLC-LIF.	
<hr/>		
Hou et al. 2009	<b>Sample Preparation, Extraction and Filtration:</b> Soil samples were air-dried, sieved and acid-vapor hydrolyzed (6 M HCl) for 12 h at 105 °C. Then, hydrolites were filtered with 2.5 M L-2-aminobutyric acid, dried and redissolved in 0.05 M HCl.	<b>HIGH</b>
	<b>Purification:</b> Purification via cation-exchange resin with washes of oxalic acid, HCl, and water. Amino acids eluted with NH <sub>4</sub> OH, then dried and redissolved in 0.1 M HC. Fianlly, the sample was centrifuged and, freeze-dried and dissolved in 0.02 M HCl.	Most amino acids were present in a <b>similar order of magnitude</b> ; an indiciative of biotic origin of these molecules.
	<b>Derivatization and separation:</b> Samples were derivatized with AQC and further analyzed via LC-MS.	
<hr/>		
Fuchida et al. 2014	<b>Extraction of hydrolyzable AAs and Filtration:</b> Sediment samples were flushed with Argon, dried and acid-vapor hydrolyzed (6 N HCl) for 22 h at 110 °C. Supernatants were filtered through a PTFE membrane.	<b>HIGH</b>
	<b>monomers and Filtration:</b> Sediment samples were flushed with Argon, dried and acid-vapor hydrolyzed (0.5 N HCl) for 24 h at RT. Supernatants were filtered through a PTFE membrane.	
	<b>Purification:</b> Purification via cation-exchange resin with washes of HCl, NaOH, and water. Amino acids eluted with NH <sub>3</sub> solution, then evaporated under vaccum at 40 °C and finally dissolved in methanol/H <sub>2</sub> O.	
	<b>Derivatization and separation:</b> Samples were derivatized with OPANAC and further analyzed via HPLC.	Low D/L ratio and abundant amounts of the <b>L-form of Glu, Asp, and Ala</b> suggest that most of the amino acids are biogenic in origin.
		<b>Low</b> amounts of amino acids <b>monomers</b> in the sediments indicated that most of the amino acids existed in polymer forms, which support the idea of mostly biogenic origin since most AAs polymers in modern marine sediments are derived from organisms and bio-debris.

**References:**

- Aerts J. W., Riedo A., Melton D. J., Martini S., Flahaut J., Meierhenrich U. J., Meinert C., Myrgorodska I., Lindner R., and Ehrenfreund P. (2020) Biosignature Analysis of Mars Soil Analogs from the Atacama Desert: Challenges and Implications for Future Missions to Mars. *Astrobiolog*
- Noell A. C., Fisher A. M., Fors-Francis K., and Sherrit S. (2018) Subcritical water extraction of amino acids from Mars analog soils. *Electrophoresis*, 39: 2854-2863.
- Hou S., He H., Zhang W., Xie H., and Zhang X. (2009) Determination of soil amino acids by high performance liquid chromatography-electro spray ionization-mass spectrometry derivatized with 6-aminoquinolyl-N-hydroxysuccinimidyl carbamate. *Talanta*, 80: 440-7.
- Fuchida S., Mizuno Y., Masuda H., Toki T., and Makita H. (2014) Concentrations and distributions of amino acids in black and white smoker fluids at temperatures over 200°C. *Organic Geochemistry*, 66: 98-106.

Dataset S7. Amino acid abundances (nmol/g) in environmental samples from the Atacama, Antarctica, grassland, and hydrothermal systems.

Amino acid	Abundance (nmol/g)																	
	Atacama								Antarctic				Grassland		Hydrothermal Systems			
	Salar Laco (ATA03)		Laguna Tuyaiblo (ATA05)		Aerts et al. 2020		Salar de Atacama (ATA15)		Noell et al. 2018		Wright Valley Soils		Hou et al. 2009		Izena Cauldron (PC1)	Fuchida et al. 2014		
D-aspartic acid	NR	NA	NR	NA	17.1	1.8	1.3	0.13										
L-aspartic acid	39.698	*	22.8467	*	73	7	4	0.4	0.98	0.23	3.85	0.29	2213	337	2158.75	NA	343.78	NA
D-glutamic acid	NR	NA	NR	NA	20	2	Below detection sensitivity	NA										
L-glutamic acid	139.3258	*	71.6233	*	174	8	19.5	1.6	3.74	0.43	8.83	0.52	1465	123	1281.97	NA	180.48	NA
D-serine	NR	NA	NR	NA	Below detection sensitivity	NA	Below detection sensitivity	NA										
L-serine	34.7016	*	38.8338	*	Limit of quantification	NA	Below detection sensitivity	NA	0.51	0.12	2.2	0.25	1328	165	1317.13	NA	492.27	NA
glycine	112.5927	*	184.0706	*	240	20	185	16	4.18	0.55	9.03	1.26	2618	97	5347.15	NA	817.96	NA
D-alanine	NR	NA	NR	NA	Limit of quantification	NA	Limit of quantification	NA	3.31	0.85	10.73	1.69	2206	242	1452.78	NA	243.36	NA
L-alanine	52.6682	*	83.4233	*	74	6	136	6										
D-valine	NR	NA	NR	NA	1.47	0.13	3.23	0.05	3.65	0.29	10.75	0.99	784	103	1775.79	NA	280	NA
L-valine	28.0825	*	21.5742	*	51	5	179	17										
D-isoleucine	NR	NA	NR	NA	0.65	0.05	2.44	0.12			7.7	0.69	332	13	875.36	NA	50.93	NA
L-isoleucine	22.8995	*	Below blank	*	20	2	96	9	1.8	0.14								
D-leucine	NR	NA	NR	NA	0.77	0.06	3.7	0.3			12.31	1.21	668	69	18.27	NA	70	NA
L-leucine	70.5916	*	27.4641	*	25	2	113	8	2.9	0.24								
D-phenylalanine	NR	NA	NR	NA	0.44	0.08	0.87	0.06			4.87	4.87	300	42	2424	NA	70	NA
L-phenylalanine	257.4771	*	7.3644	*	9.7	0.7	33	3	0.14	0.04								
D-threonine	NR	NA	NR	NA	NR	NA	NR	NA			4.44	0.33	1123	156	1040.4	NA	202.64	NA
L-threonine	35.2993	*	22.2787	*	NR	NA	NR	NA	1.71	0.11								
D,L-proline	NR	NA	NR	NA	27.7	1.6	37.6	1.1	1.66	0.24	4.43	0.64	828	86	NR	NA	NR	NA
D,L-tyrosine	NR	NA	NR	NA	NR	NA	NR	NA	0	0.06	0.55	0.12	76	9	BD	NA	BD	NA
D, L-lysine	NR	NA	NR	NA	NR	NA	NR	NA	0.8	0.14	0.95	0.18	989	97	812.73	NA	110	NA

\* Measurement uncertainty of 10% is applied  
 NR: Not reported  
 BD: Below detection